Homogenization-based multiscale crack modelling: from micro diffusive damage to macro cracks

Vinh Phu Nguyen [1,*], Oriol Lloberas-Valls[2,*], Martijn Stroeven[3,*], Lambertus Johannes Sluys[4,*]

Delft University of Technology, Faculty of Civil Engineering and Geosciences, P.O. Box 5048, 2600 GA Delft, The Netherlands

Abstract

The existence of a representative volume element (RVE) for a class of quasi-brittle materials having a random heterogeneous microstructure in tensile, shear and mixed mode loading is demonstrated by deriving traction-separation relations, which are objective with respect to RVE size. A computational homogenization based multiscale crack modelling framework, implemented in an FE^2 setting, for quasi-brittle solids with complex random microstructure is presented. The objectivity of the macroscopic response to the micro sample size is shown by numerical simulations. Therefore, a homogenization scheme, which is objective with respect to macroscopic discretization and microscopic sample size, is devised. Numerical examples including a comparison with direct numerical simulation are given to demonstrate the performance of the proposed method.

Keywords: representative volume element (RVE), quasi-brittle materials, softening, multiscale, homogenization, cohesive law, fracture

1. Introduction

The majority of natural and engineering materials are materials in which deformation and failure processes take place at multiple scales and are therefore called multiscale materials (by multiscale we mean multiple length scales). At the macroscopic level of observation, it is reasonable to consider materials as homogeneous, traditionally modelled by phenomenological constitutive laws. At lower observation levels (meso and/or micro) heterogeneities appear which are very troublesome to be taken into account in phenomenological constitutive models. There are three approaches by which heterogeneous materials can be modelled. The first approach is known as either direct numerical simulation (DNS) or brute-force fullscale simulation, in which the heterogeneities from the fine scale are explicitly modelled in the coarse scale model. Although this guarantees accuracy, the computational effort is impractical (at least for current computer technology) which limits the applicability of the DNS approach. The second approach is based on the homogenization concept and has emerged as a valuable tool to model heterogeneous materials in an efficient way. The third approach, known as the concurrent multiscale method, somehow resemble domain decomposition methods. For a detailed taxonomy of multiscale methods, refer to [1].

---

*Corresponding author
[1]V.P.Nguyen@tudelft.nl
[2]O.LloberasValls@tudelft.nl
[3]M.Stroeven@tudelft.nl
[4]L.J.Sluys@tudelft.nl

Homogenization-based multiscale modelling techniques can either be numerical homogenization [2] or computational homogenization [3], see [4] for a detailed discussion. In numerical homogenization schemes, a macroscopic canonical constitutive model e.g., a visco-plasticity model, is assumed with parameters determined by fitting the data produced by finite element (or any other numerical method) computations of a microscopic sample where all the microstructure is explicitly modelled. In the literature, those numerical homogenization techniques are known as unit cell methods. Due to the assumption of the form of the macroscopic constitutive law, the methods become less appropriate for highly nonlinear problems.

According to computational homogenization techniques, to every macroscopic material point there is an associated microscopic sample (with all relevant heterogeneities) which provides the macroscopic constitutive behavior. When implemented in a finite element (FE) framework, the method is known as an FE^2 [5] scheme. Although the method is computationally expensive, it has been proved to be a valuable and flexible (due to the lack of an assumption on the macroscopic constitutive model) tool for analyzing a wide range of heterogeneous materials with complex microstructures with highly nonlinear behavior see, among others, [6, 7, 8] and [9] for a recent review. An open source program for homogenization problems has recently been made available [10].

A concept of crucial importance in homogenization methods is the representative volume element (RVE). There is not a single and exact definition of the RVE for an arbitrary heterogeneous material. That might explain the existence of various definitions of the RVE, see [11] for a recent review. In this contribution, we consider a microscopic sample to be an RVE when *(i)* an increase in its size does not lead to considerable differences in the homogenized properties, *(ii)* the micro sample size is large enough so that the homogenized properties are independent of the microstructural randomness and *(iii)* the RVE size should be small enough that the separation-of-scales principle holds. An implicit assumption usually made in FE^2 modelling is the existence of an RVE. This is a correct assumption in linear and hardening regimes [11]. However, this is no longer the case in softening regimes when a standard homogenization method is used [11].

In the past two years homogenization schemes for adhesive cracks (or material layers) [12, 13, 14, 15] and cohesive cracks [16, 17] have been developed in which a traction-separation law is obtained based upon finite element computations at the microscale wherein the complex microstructure of the material have been explicitly modelled. By doing homogenization for adhesive cracks, in [14] the existence of an RVE for softening materials (under tensile and mixed-mode loading) which exhibit diffusive damage has been reported. The same result has been recently presented in [15] for fibre-epoxy material that shows discrete cracking. Very recently, in [17] the authors have proved the existence of an RVE for softening materials, for both adhesive and cohesive cracks, by deriving a traction-separation law from the microscopic inelastic stresses and strains. However the method has been applied only to materials with a simple microstructure undergoing discrete cracking.

In [18, 1], the authors have developed the MAD (Multiscale Aggregating Discontinuities) method in which a macroscopic crack is determined as equivalent to a bunch of microscale cracks. The method is however restricted to cases where the separation-of-scales principle is violated for the micro sample had to match the macro element to which it is linked. Computational multiscale methods to model cracks wherein the microstructural length scale is of the same magnitude as the macroscopic length scale are also given in [19, 20].

In [21], the existence of an RVE for quasi-brittle materials (under tensile loading) with random complex heterogeneous microstructure exhibiting diffusive damage has been confirmed based upon a special averaging scheme, the failure zone averaging scheme, which filters out the linear contribution of the micro sample.

In this manuscript departing from the result reported in [21], we are going to derive cohesive laws, which are objective with respect to micro sample size, for softening materials with a random heterogeneous microstructure subjected to tensile, shear and mixed-mode loading. It is confirmed that an RVE does exist for softening materials with microstructures undergoing diffusive damage. We also present a computational framework to incorporate those objective cohesive laws in an iterative FE^2 setting which is an extension of the approach given in [17] for micro discrete cracking failure to micro diffusive damage fracture. Although similar in some aspects, the major difference between

our work and [17] is two-fold. Firstly, the microstructure in this paper exhibits diffusive damage i.e., we homogenize a macroscopic cohesive law from a microscale localization band. Secondly, the representativeness of the macroscale cohesive law is obtained for materials with a random microstructure and under various loading conditions.

The structure of the paper is as follows. In Section 2, the investigated microstructures and the utilized continuum damage model are given. Section 3 presents the standard averaging scheme, the proposed failure zone averaging technique followed by a series of numerical simulations that confirm the existence of an RVE for softening materials. The next section, section 4, describes the energetic equivalence theorems to link macroscopic and microscopic models. The multiscale algorithm for adhesive and cohesive cracks is given in Section 5 followed by three numerical examples given in Section 6.

2. Microstructures and Constitutive model
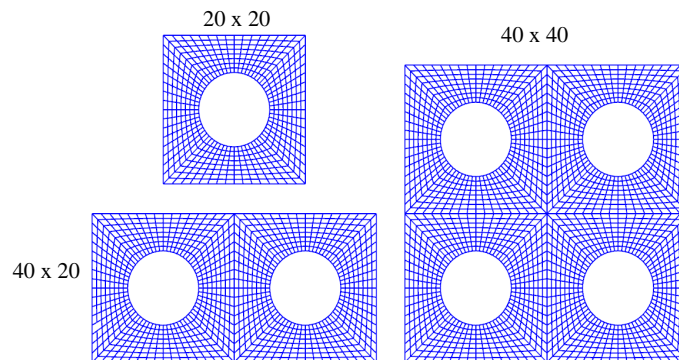
2.1. Microstructures

Figure 1: Investigated three unit cells made of regular microstructure. All units are in mm.

In this paper, two microstructures are considered. The first one is a simple voided microstructure (radius of the void equals 5 mm) of which three samples with dimensions 20×20 mm^2, 40×20 mm^2 and 40×40 mm^2 as shown in Fig.(1) will be studied. The second type of microstructure that is analyzed in this contribution is a random heterogeneous material which is a three-phase material with matrix, aggregates and an interfacial transion zone (ITZ) surrounding each aggregate, see Fig.(2). Two samples of dimensions 15×15 mm^2 and 20×20 mm^2, as shown in Fig.(3), corresponding to 45% aggregate volume fraction are investigated. Details on the generation procedure of these samples can be found in [22]. Note that we have not considered bigger samples and different realizations since a statistical analysis of the existence of an RVE for this kind of material has already been given in [21].

2.2. Constitutive model

Damage of the samples is modelled by a simple isotropic damage model regularized by the gradient enhanced method [23]. For sake of completeness, this model is briefly summarized here. The stress-strain relation is given by [24]

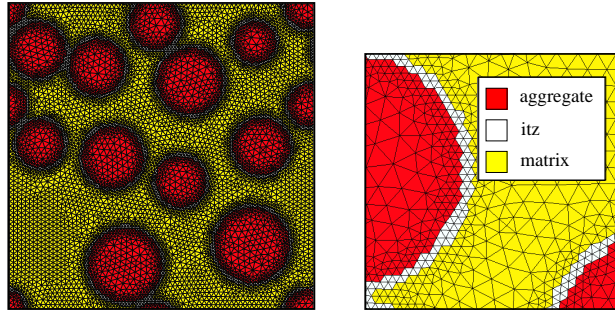$$\boldsymbol{\sigma} = (1 - \omega)\mathbf{D}_e : \boldsymbol{\epsilon} \tag{1}$$

3

Figure 2: Finite element mesh of the three-phase material sample: full view (left) and close-up view (right).

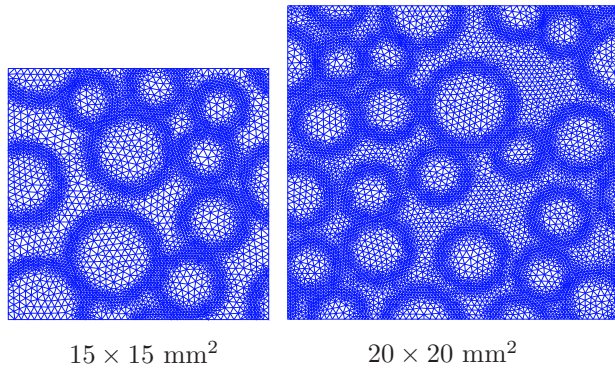15×15 mm^2 20×20 mm^2

Figure 3: Two micro samples of random heterogeneous material (45% aggregate).

where ω is the scalar damage variable and the fourth order tensor $\mathbf{D}_e$ contains the elastic moduli. Damage is governed by the following exponential law

$$\omega = 1 - \frac{\kappa}{\kappa_I}[1 - \alpha + \alpha \exp^{-\beta(\kappa - \kappa_I)}], \quad \kappa \geq \kappa_I \tag{2}$$

where α (residual stress), β (softening slope) and κ_I (damage threshold) denote the inelastic parameters. The variable κ is the largest nonlocal equivalent strain $\bar{\epsilon}_{eq}$ ever reached. The nonlocal equivalent strain is defined according to an implicit gradient enhanced damage formulation given in [23]

$$\bar{\epsilon}_{eq} - c\nabla^2\bar{\epsilon}_{eq} = \epsilon_{eq} \tag{3}$$

in which ϵ_{eq} is the Mazars local equivalent strain [25] and c is a positive valued parameter of dimension length squared.

For the voided microstructure, the material parameters include a Young's modulus E of 25000 MPa, Poisson's ratio ν of 0.2, damage threshold κ_I of 3×10^{-5}, $\alpha = 0.999$, $\beta = 5000$ and $c = 3.5$ mm^2. For the heterogeneous material, the material parameters are given in table 1.

		Matrix	Aggregate	ITZ
E	[N/mm^2]	25000	30000	20000
ν	[-]	0.2	0.2	0.2
κ_I	[-]	5e-06	0.5	3e-06
α	[-]	0.999	0.999	0.999
β	[-]	1500	1500	1500
c	mm^2	0.2	0.2	0.2

Table 1: Material parameters of different phases of the random heterogeneous material.
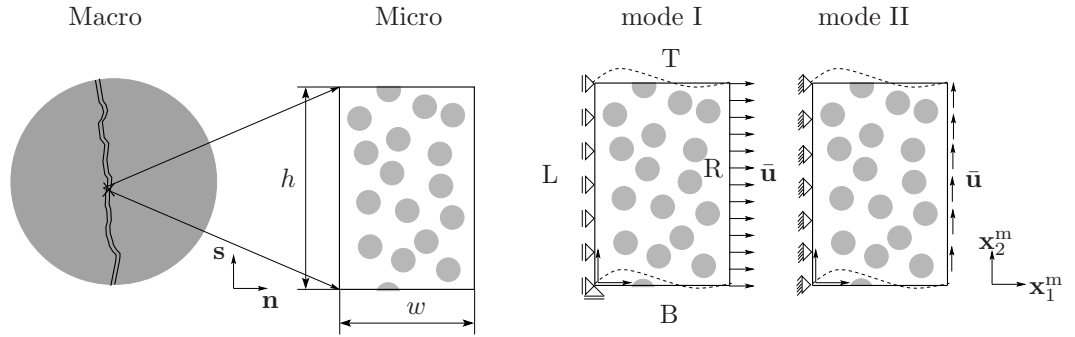
3. Objective macroscopic cohesive laws

Figure 4: From left to right: macro sample with a crack, micro model, boundary conditions for tensile and shear loading. Periodic boundary conditions on the bottom and top edges are denoted by dashed lines. Material periodicity is also considered.

Considering a macro crack with the outward unit normal denoted by $\mathbf{n}$ and the unit tangent vector represented by $\mathbf{s}$. A micro sample Ω_m, which is a rectangle of dimension $w \times h$, wherein the underlying microstructure is explicitly

modelled is associated to every integration point on the macro crack. Let us consider the case in which $\mathbf{n}$ coincides with $\mathbf{x}_1^{\mathrm{m}}$ see Fig.(4) for the microscale orthogonal coordinate system. Since the deformation modes of the macro crack include mode I opening and mode II shearing, the boundary conditions (BCs) of the micro model are the ones given in Fig.(4) for mode I and mode II cases. For mixed-mode problems, BCs are the combination of BCs of mode I and mode II. The external boundary of the micro sample is denoted by Γ_{m} which is composed of Γ_{T}, Γ_{B}, Γ_{L} and Γ_{R}.

3.1. Standard averaging techniques

The macroscopic homogenized stress $\boldsymbol{\sigma}_{\mathrm{M}}$ is given by see [26]

$$
\begin{aligned}
\boldsymbol{\sigma}_{\mathrm{M}} &\equiv \frac{1}{wh} \int_{\Omega_{\mathrm{m}}} \boldsymbol{\sigma}_{\mathrm{m}} \mathrm{d}\Omega = \frac{1}{wh} \int_{\Gamma_{\mathrm{m}}} \mathbf{t}_{\mathrm{m}} \otimes \mathbf{x}_{\mathrm{m}} \mathrm{d}\Gamma \\
&= \frac{1}{wh} \int_{\Gamma_{\mathrm{R}}} \mathbf{t}_{\mathrm{m}} \otimes (\mathbf{x}_{\mathrm{R}} - \mathbf{x}_{\mathrm{L}}) \mathrm{d}\Gamma + \frac{1}{wh} \int_{\Gamma_{\mathrm{T}}} \mathbf{t}_{\mathrm{m}} \otimes (\mathbf{x}_{\mathrm{T}} - \mathbf{x}_{\mathrm{B}}) \mathrm{d}\Gamma
\end{aligned}
\tag{4}
$$

where use was made of the anti-periodicity of the tractions. In this manuscript, subscripts $\square_{\mathrm{M}}$ and $\square_{\mathrm{m}}$ are used to indicate if a quantity belongs to the macro or micro scale, respectively. The micro stress tensor, traction vector and position vector are denoted by $\boldsymbol{\sigma}_{\mathrm{m}}$, $\mathbf{t}_{\mathrm{m}}$ and $\mathbf{x}_{\mathrm{m}}$, respectively. Quantities associated to the top, bottom, left and right edges of the micro sample are indicated by subscripts T, B, L and R, respectively, see Fig.(4).

By using the following relations

$$
\mathbf{x}_{\mathrm{R}} - \mathbf{x}_{\mathrm{L}} = w\mathbf{n}, \quad \mathbf{x}_{\mathrm{T}} - \mathbf{x}_{\mathrm{B}} = h\mathbf{s}
\tag{5}
$$

Equation (4) becomes

$$
\boldsymbol{\sigma}_{\mathrm{M}} = \frac{1}{h} \int_{\Gamma_{\mathrm{R}}} \mathbf{t}_{\mathrm{m}} \mathrm{d}\Gamma \otimes \mathbf{n} + \frac{1}{w} \int_{\Gamma_{\mathrm{T}}} \mathbf{t}_{\mathrm{m}} \mathrm{d}\Gamma \otimes \mathbf{s}
\tag{6}
$$

Adopting the fact that $\mathbf{n}^{\mathrm{T}} = (1, 0)$ and $\mathbf{s}^{\mathrm{T}} = (0, 1)$, the above is simplified to

$$
\boldsymbol{\sigma}_{\mathrm{M}} = \begin{bmatrix} \dfrac{f_{\mathrm{R,x}}^{\mathrm{int}}}{h} & \dfrac{f_{\mathrm{T,x}}^{\mathrm{int}}}{w} \\ \dfrac{f_{\mathrm{R,y}}^{\mathrm{int}}}{h} & \dfrac{f_{\mathrm{T,y}}^{\mathrm{int}}}{w} \end{bmatrix}
\tag{7}
$$

where $\mathbf{f}_{\mathrm{R}}^{\mathrm{int}}$ and $\mathbf{f}_{\mathrm{T}}^{\mathrm{int}}$ are the sum of nodal internal forces along the right and top edges, respectively. Note that the homogenized stress tensor is symmetric due to the rotational equilibrium of the micro sample i.e., $w f_{\mathrm{R,y}}^{\mathrm{int}} = h f_{\mathrm{T,x}}^{\mathrm{int}}$.

The homogenized strain tensor $\boldsymbol{\epsilon}_{\mathrm{M}}$ is given by see [26]

$$
\boldsymbol{\epsilon}_{\mathrm{M}} \equiv \frac{1}{wh} \int_{\Omega_{\mathrm{m}}} \boldsymbol{\epsilon}_{\mathrm{m}} \mathrm{d}\Omega = \frac{1}{wh} \int_{\Gamma_{\mathrm{m}}} (\mathbf{u}_{\mathrm{m}} \otimes^{\mathrm{sym}} \mathbf{n}) \mathrm{d}\Gamma
\tag{8}
$$

where the divergence theorem was used to convert the domain integral to a surface integral. The operator $\otimes^{\mathrm{sym}}$ denotes the symmetrized dyadic product. The micro strain tensor and the displacement vector are represented by $\boldsymbol{\epsilon}_{\mathrm{m}}$ and $\mathbf{u}_{\mathrm{m}}$, respectively.

The above can be more elaborated as

$$\boldsymbol{\epsilon}_{\mathrm{M}} = \frac{1}{wh} \left\{ \int_{\Gamma_{\mathrm{T}}} [(\mathbf{u}_{\mathrm{T}}^{\mathrm{m}} - \mathbf{u}_{\mathrm{B}}^{\mathrm{m}}) \otimes^{\mathrm{sym}} \mathbf{s}] \, \mathrm{d}\Gamma + \int_{\Gamma_{\mathrm{R}}} [(\mathbf{u}_{\mathrm{R}}^{\mathrm{m}} - \mathbf{u}_{\mathrm{L}}^{\mathrm{m}}) \otimes^{\mathrm{sym}} \mathbf{n}] \, \mathrm{d}\Gamma \right\}$$
$$= \frac{1}{h} \bar{\mathbf{u}} \otimes^{\mathrm{sym}} \mathbf{s} + \frac{1}{w} \bar{\mathbf{u}} \otimes^{\mathrm{sym}} \mathbf{n} \tag{9}$$

where use has been made of the periodicity of the displacement field in the last equality. In matrix form, the homogenized strain tensor is given by

$$\boldsymbol{\epsilon}_{\mathrm{M}} = \begin{bmatrix} \dfrac{\bar{u}_x}{w} & \dfrac{1}{2}\left(\dfrac{\bar{u}_x}{h} + \dfrac{\bar{u}_y}{w}\right) \\ \mathrm{sym.} & \dfrac{\bar{u}_y}{h} \end{bmatrix} \tag{10}$$

The macroscopic traction vector $\mathbf{t}_{\mathrm{M}}$ is assumed to be the projection of the macroscopic stress tensor on the crack plane [13, 17]. That is

$$\mathbf{t}_{\mathrm{M}} \equiv \boldsymbol{\sigma}_{\mathrm{M}} \cdot \mathbf{n} = \frac{\mathbf{f}_{\mathrm{R}}^{\mathrm{int}}}{h} \tag{11}$$

where use was made of Eq.(7).

The homogenized stress-strain $(\sigma_{\mathrm{M}}^x, \epsilon_{\mathrm{M}}^x)$ curves as well as the traction-displacement $(t_{\mathrm{M}}^x, \bar{u}_x)$ diagrams of the three voided samples (see Fig.(1)) subjected to a tensile loading are given in Fig.(5). The result on the left shows that for bulk homogenization, the linear elastic response is objective to the micro model size (due to the fact that the elastic slope of the stress-strain curves is the Young's modulus E in one dimension) and the softening branches are, however, micro model size dependent. For a complete analysis on the sample size dependency of the homogenized stress-strain diagrams for quasi-brittle materials with a random microstructure, see [11]. On the contrary, for interface homogenization [15, 14][5], the linear response is inversely proportional to the width of the sample i.e., being E/w for one dimensional problems. Obviously, both bulk and interface homogenizations based on standard averaging theorems give results which are not objective to the micro sample size. Figure (6) shows the damage distribution in the samples.

Remark 3.1. We have introduced a numerical imperfection to trigger localization at the left voids in samples 40×20 mm² and 40×40 mm², see Fig.(6). Note that our target material is a brittle random heterogeneous material, Fig.(2), of which failure is accompanied with the occurrence of one propagating localization band, see Fig.(7) (no numerical imperfection is needed here). The voided microstructure merely serves as an exemplary material to illustrate our ideas with very low computational cost. The introduction of artificial imperfections for voided samples is just to mimic the behaviour of real random heterogeneous materials. Note that the 40×20 mm² and 40×40 mm² samples have the same bifurcated solutions, thus the same homogenized response and the 20×20 mm² sample captures a different bifurcated path, thus a different homogenized response, Fig.(5). However, as demonstrated in [21] (see also Fig.(8)b), the homogenized macroscopic response is size-independent when a proper averaging technique is used even though the samples follow different bifurcation paths. The discussion of bifurcated solutions at the microscale is beyond the scope of this manuscript. Refer to [27] for a related discussion.

---

[5]By interface homogenization, the homogenized quantities are the traction and the displacement of the right edge.
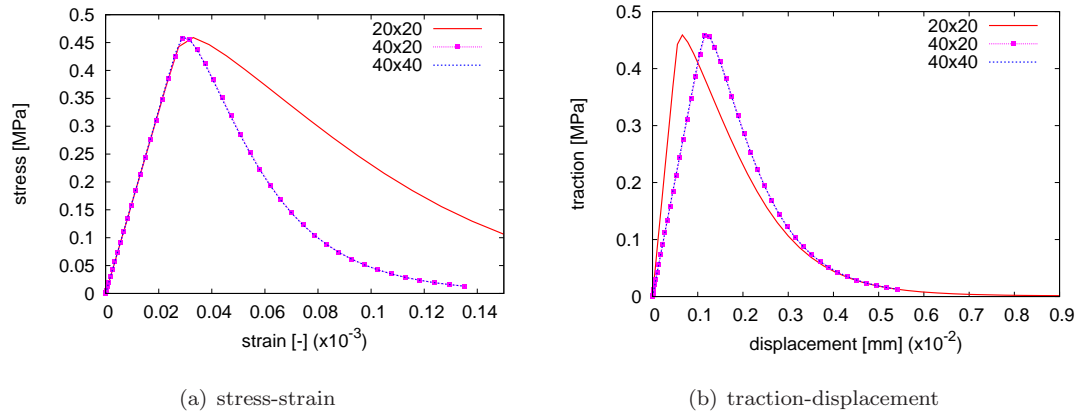
(a) stress-strain

(b) traction-displacement

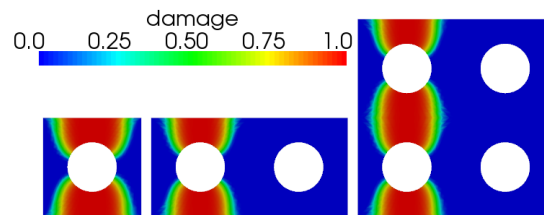Figure 5: Three voided samples in tension: bulk vs interface homogenization.

Figure 6: Damage patterns of three samples under horizontal tensile loading.

3.2. Failure zone averaging technique

In [21], the authors have proposed a special averaging scheme which was named *failure zone averaging scheme* with which the existence of an RVE for random heterogeneous quasi-brittle materials in softening regime has been proved. For the sake of completeness, this averaging scheme is described shortly. Let us first denote Ω_d as the active damaged domain i.e., the region containing Gauss points which are damaged and loading. According to the continuum damage model, this domain corresponds to Gauss points satisfying $\kappa > \kappa_I$ and $f = 0$ (f is the loading function), see Fig.(7) for a graphical illustration. We define the homogenized stresses and strains as the volume averages of the microscopic stresses and strains, respectively, over Ω_d rather than over Ω_m

$$
\begin{aligned}
\langle \boldsymbol{\sigma} \rangle_{\text{dam}} &= \frac{1}{|\Omega_d|} \int_{\Omega_d} \boldsymbol{\sigma}_m d\Omega_d \\
\langle \boldsymbol{\epsilon} \rangle_{\text{dam}} &= \frac{1}{|\Omega_d|} \int_{\Omega_d} \boldsymbol{\epsilon}_m d\Omega_d
\end{aligned}
\tag{12}
$$

where $|\cdot|$ denotes the measure of the domain. Since the above domain integrals cannot be converted to surface integrals along Γ_m[6], they are computed directly using numerical quadrature. This averaging will filter out the linear contribution which makes the standard stress-strain diagrams micro-sample size dependent.
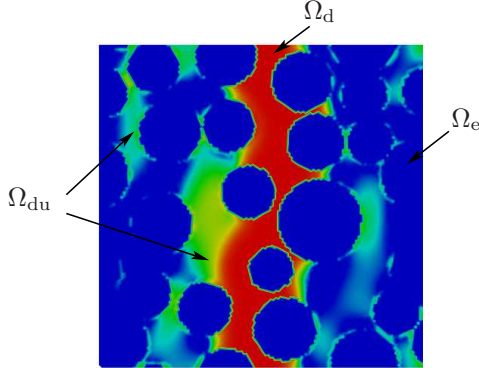

Figure 7: Definition of the damage domain Ω_d over which the averages are performed: $\Omega_d = \Omega_m \setminus \Omega_e(\text{elastic}) \setminus \Omega_{du}(\text{unloading damaged})$.

In Fig.(8) the homogenized stress-strain diagrams of the three voided samples (see Fig.(1)) obtained with the standard averaging scheme (left) and the new failure zone averaging method (right) are given. Figure (8a) clearly demonstrates that for softening regime there is no unique size of an RVE- a result reported in [28, 11]. However, Fig.(8b) shows that the stress-strain curves are independent of the micro sample size which in turn means that there exists an RVE for softening materials if the stresses and strains have been defined using the proposed failure zone averaging. Note that the absence of a linear branch in the presented curves is due to the fact that the failure zone averaging should only be used after development of a failure band. Based on this observation plus a statistical analysis presented in [21], the authors have confirmed the existence of an RVE for quasi-brittle materials with random heterogeneous microstructure that exhibit localized failure with a continuum damage model.

---

[6]Note that using standard averaging, see section 3.1, the homogenized quantities are directly related to the micro quantities on the boundary.
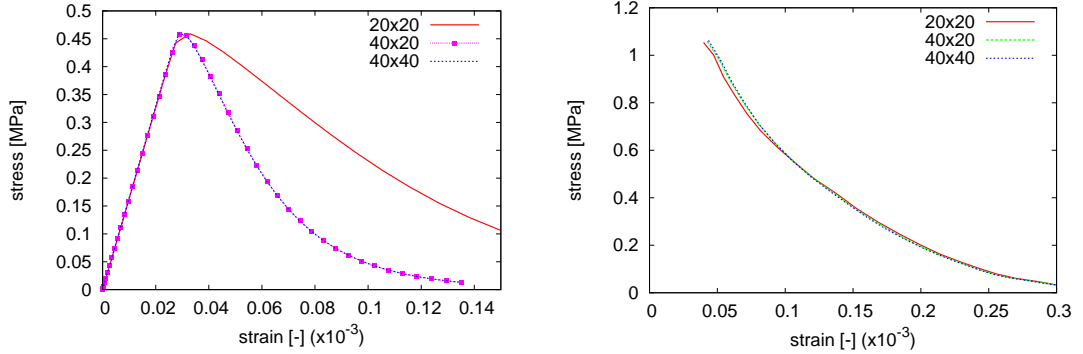
Figure 8: Responses of micro samples of regular microstructure obtained with the standard averaging (left) and the failure zone averaging (right).

3.3. Traction-separation law

In the previous section we have shown that, by performing the averaging over the active damaged domain Ω_{d}, homogenized stress-strain curves can be obtained which are objective with respect to micro sample size. In what follows, we are going to present a method to extract a macroscopic cohesive law from the microscopic response in the active damaged domain which is independent of the micro sample size.

To this end, let us first define the displacements due to damage $\mathbf{u}_{\mathrm{dam}}$ as follows

$$\mathbf{u}_{\mathrm{dam}} = \langle \boldsymbol{\epsilon} \rangle_{\mathrm{dam}} \cdot (l\mathbf{n}) \tag{13}$$

where l is the averaged width of the localization band which is equal to $|\Omega_{\mathrm{d}}|\,/h$, see section 4 for the definition of l.

Figure (9) plots the traction versus the damage opening $(t_{\mathrm{M}}^{x}, u_{\mathrm{dam}}^{x})$ curves[7] for the three voided samples in tension which are obviously independent of the sample sizes. It should be noticed that this conclusion applies only for the portion of the curves after the peak. We therefore define the macro crack opening $[\![\mathbf{u}]\!]_{\mathrm{M}}$ as the damage opening $\mathbf{u}_{\mathrm{dam}}$ shifted to the left by an amount of $\mathring{\mathbf{u}}_{\mathrm{dam}}$ which is the damage opening corresponding to the maximum traction

$$[\![\mathbf{u}]\!]_{\mathrm{M}} = \mathbf{u}_{\mathrm{dam}} - \mathring{\mathbf{u}}_{\mathrm{dam}} \tag{14}$$

to obtain initially rigid macroscopic traction-opening relations.

Figure (10) reveals the fact that the traction-opening $(t_{\mathrm{M}}^{x}, [\![u]\!]_{\mathrm{M}}^{x})$[8] relation is unique regardless of the sample size which is a result recently reported by [17] for microstructures exhibiting discrete cracking. Note the similarity of Eq.(14) with equation (19) in [17] that defines the macro opening displacement as the non-elastic part of the micro displacement. However the result here holds for a continuum damage model which is relevant for many softening materials.

At first glance this result might seem surprising since the traction $\mathbf{t}_{\mathrm{M}}$ reflects the tensile stress level at the whole micro sample while the failure displacement $\mathbf{u}_{\mathrm{dam}}$ is only evaluated at the area of damage growth. Nevertheless, it can be explained in a rigorous manner by a proper energetic equivalence theorem which is given in section 4.

---

[7]The traction-displacement diagrams, already shown in Fig.(5), are re-given here to compare interface homogenization with the proposed scheme.

[8]We have shown again the $(t_{\mathrm{M}}^{x}, u_{\mathrm{dam}}^{x})$ curves already presented in Fig.(9) so that the procedure from $\mathbf{u}_{\mathrm{dam}}$ to $[\![\mathbf{u}]\!]_{\mathrm{M}}$ can be easily followed.
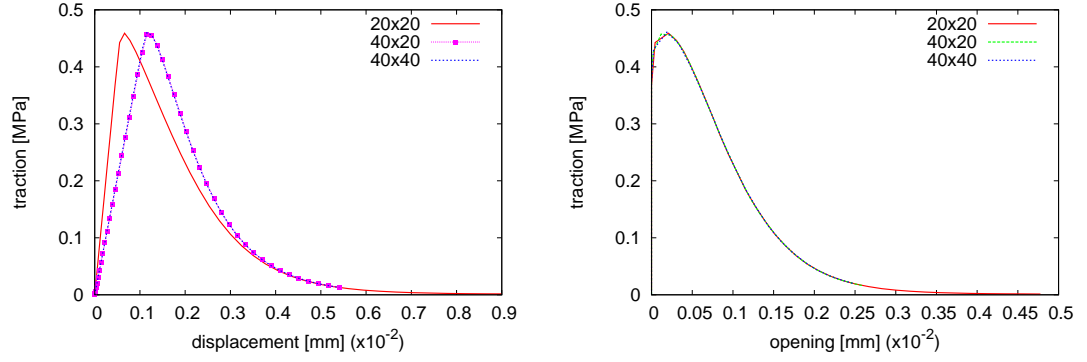
10

Figure 9: Three voided samples in tension: traction vs. applied displacement (left) and traction vs. normal damage displacement u_{dam}^{x} (right).
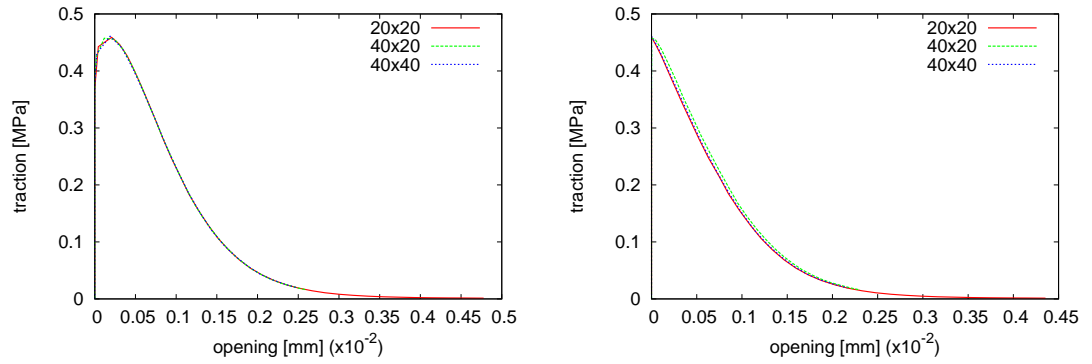

Figure 10: Traction vs. crack opening displacement diagrams. Left: standard one (computed directly from Eq.(13)) and right, shifted one obtained with Eq.(14).

11

3.4. Samples under shear and mixed mode loading

The above analysis is repeated now for the three voided samples (see Fig.(1)) under shear loading, refer to Fig.(11) for the damage distribution on the deformed configuration. The result for shear loading is given in Fig.(12) in which the top figures show results corresponding to the standard averaging scheme whereas the bottom figures show the responses obtained with the failure zone averaging scheme. It is observed once again that using the standard averaging technique, both stress-strain (bulk homogenization) and traction-separation (crack homogenization) diagrams are sample size dependent. On the contrary, when the failure zone averaging scheme is used, both the stress-strain and traction-separation curves are independent of the sample size or equivalently an RVE does exist for softening materials under shear loading.
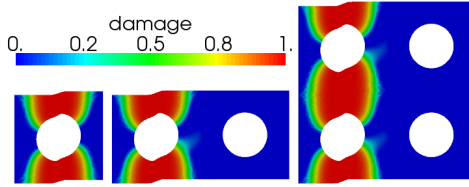

Figure 11: Damage patterns of three voided samples under shear loading (magnification factor of 50).

Next, mixed mode loading (a displacement $(\bar{u}_x, \bar{u}_y)$ was imposed on the right edge of the micro sample) has also been performed for these three samples of which the result is given in Fig.(13) wherein the first row shows the result of mode I whereas the second row gives the behavior of mode II. It is observed once again that the traction-separation curves are independent of the sample size.

3.5. Existence of an RVE for materials with random microstructure

The analysis is finally applied to the two samples with random complex microstructure, see Fig.(3), for both tensile and shear loading conditions. The results given in Fig.(14) and Fig.(15) confirm the independence of the homogenized response with respect to the sample size if the failure zone averaging was used to extract only the inelastic responses occurring in the samples. Please refer to [21] for a statistical study on the existence of an RVE for this material under a tensile loading condition. For shear loading further studies for more samples in combination with a statistical analysis would be necessary to prove the applicability of the proposed averaging technique. In Fig.(16) typical damage patterns in the samples are given.

4. Energetic equivalence theorem

Fracture can occur inside the bulk of the material or along the interface between two different materials. For the former, the fracture surface is termed a cohesive crack whereas for the latter, the term adhesive (or interfacial) crack is used. For the case of cohesive cracks, homogenization is applied to a finite element model representing the bulk material around the crack. In the case of adhesive cracks, the adopted micro model represents the material in the adhesive layer. This section develops the link between macro and micro models for both cohesive and adhesive cracks.

4.1. Cohesive cracks

In section 3.2 the objectivity of the $(\langle\boldsymbol{\sigma}\rangle_{\mathrm{dam}}, \langle\boldsymbol{\epsilon}\rangle_{\mathrm{dam}})$ curves has been demonstrated via numerical experiments. We have shown that the $(\mathbf{t}_{\mathrm{M}}, \mathbf{u}_{\mathrm{dam}})$ diagrams are independent of the micro sample size as well. In what follows, we are going to prove mathematically the representativeness of $(\mathbf{t}_{\mathrm{M}}, \mathbf{u}_{\mathrm{dam}})$ diagrams providing the objectivity of $(\langle\boldsymbol{\sigma}\rangle_{\mathrm{dam}}, \langle\boldsymbol{\epsilon}\rangle_{\mathrm{dam}})$

(a) Stress-strain

(b) Traction-displacement

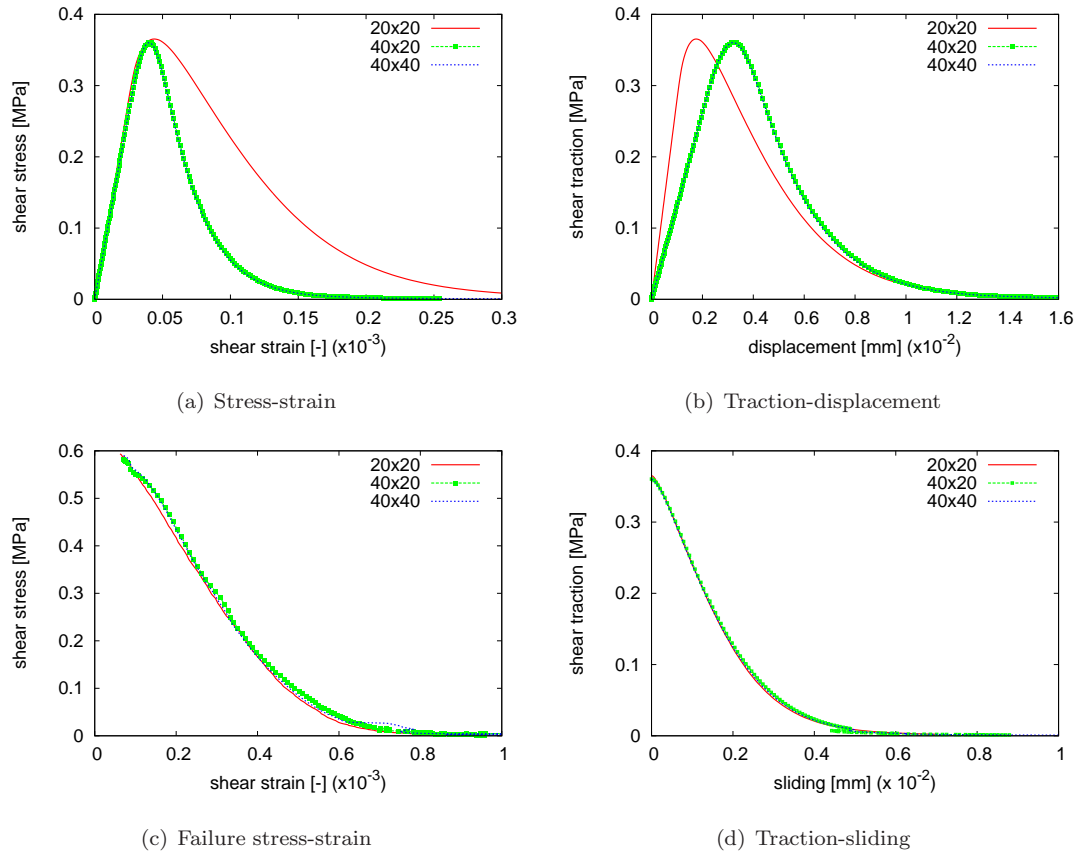(c) Failure stress-strain

(d) Traction-sliding

Figure 12: Behaviour of three voided samples under shear loading. In the first row, standard homogenization for bulk and crack whereas in the second row, failure zone averaging scheme for bulk and crack.
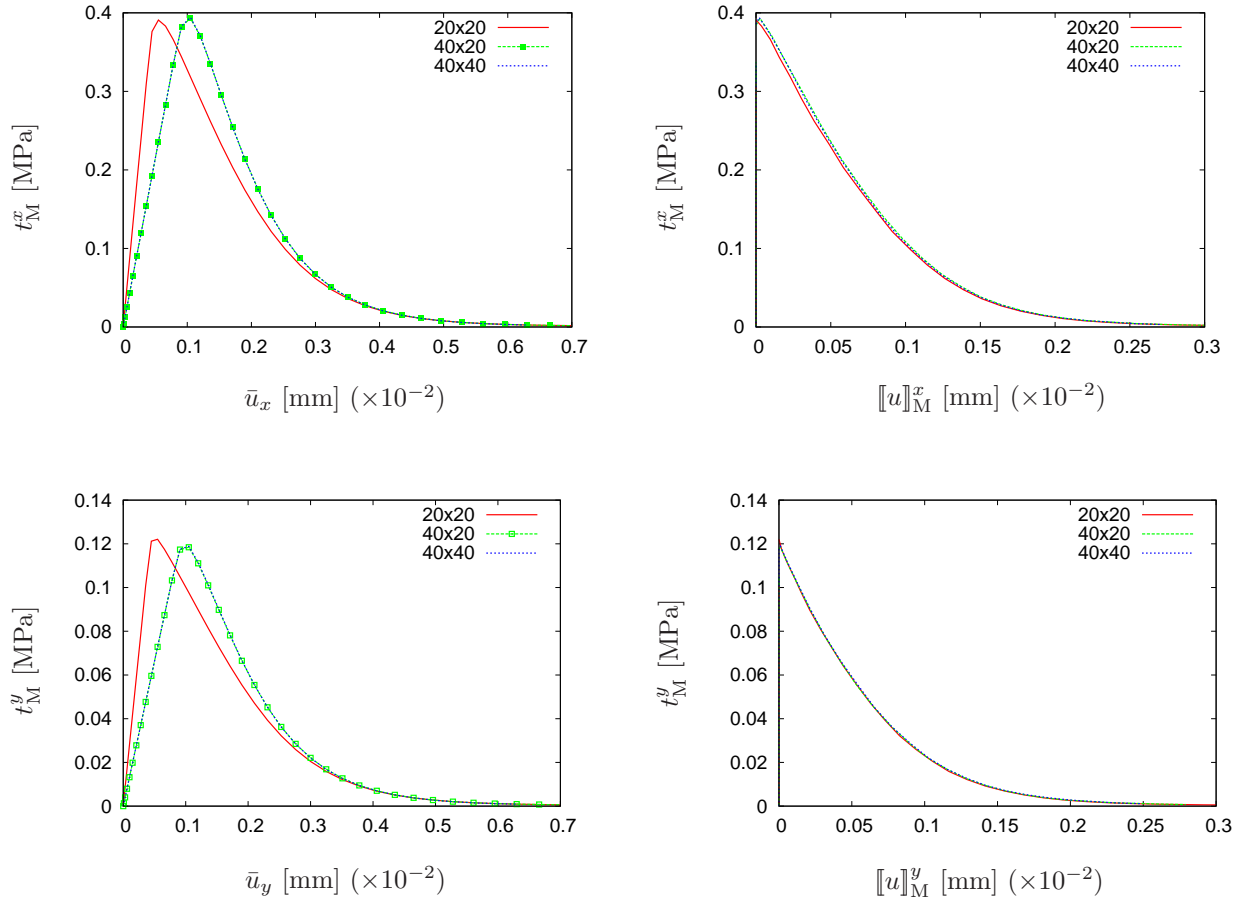
13

Figure 13: Three voided samples under mixed mode loading: standard averaging versus failuze zone averaging, for x-component (top) and for y-component (bottom).
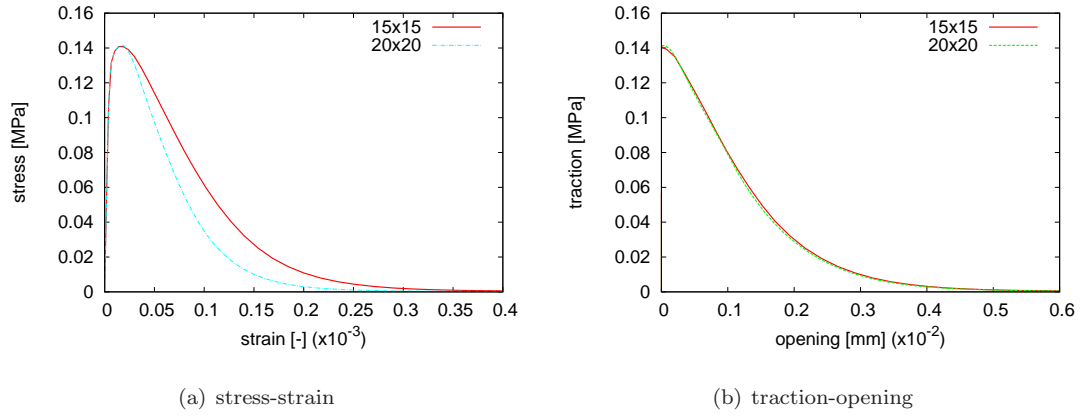
(a) stress-strain

(b) traction-opening

Figure 14: Bulk versus crack homogenization for random microstructure under tensile loading.

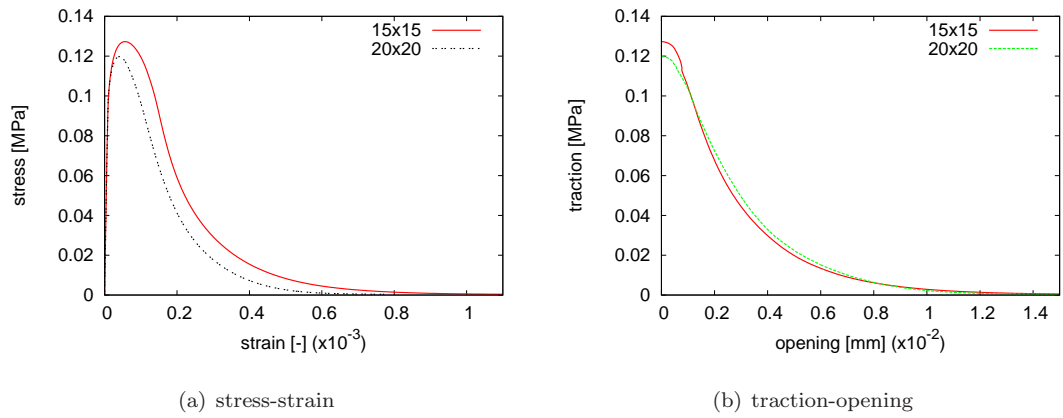(a) stress-strain

(b) traction-opening

Figure 15: Bulk versus crack homogenization for random microstructure under shear loading.
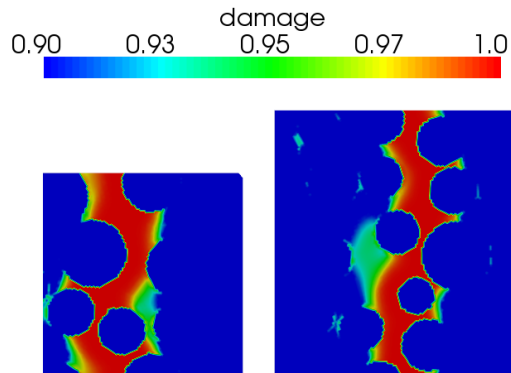

Figure 16: Damage patterns in random heterogeneous samples under tension. Note that the failure bands are periodic.
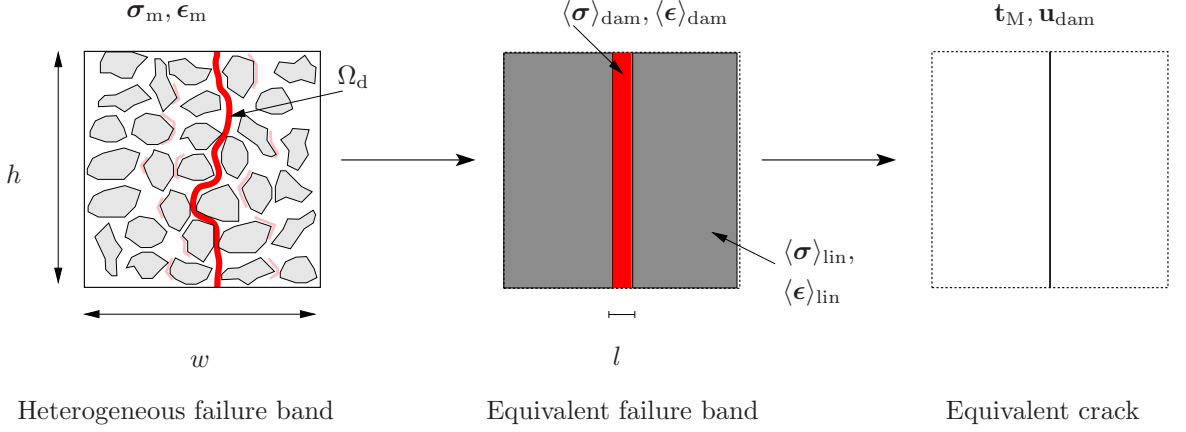
15

Figure 17: From localization band to equivalent crack via energetic equivalence consideration.

curves (which have been demonstrated extensively in [21], see also Fig.(8)). To this end, we need to prove the following equation

$$\langle \boldsymbol{\sigma} \rangle_{\mathrm{dam}} : \langle \boldsymbol{\epsilon} \rangle_{\mathrm{dam}} lh = \mathbf{t}_{\mathrm{M}} \cdot \mathbf{u}_{\mathrm{dam}} h \tag{15}$$

where the left hand side is the energy dissipated in the active damage zone Ω_{d} and the right hand side is the dissipated energy of the equivalent macro crack. Note that l is the width of the equivalent failure band which is equal to $|\Omega_{\mathrm{d}}| / h$, see Fig.(17).

The proof of the above is as follows. The right hand side of the above equation can be elaborated as

$$\begin{aligned}
\mathbf{t}_{\mathrm{M}} \cdot \mathbf{u}_{\mathrm{dam}} h &= [\langle \boldsymbol{\sigma} \rangle_{\mathrm{dam}} \cdot \mathbf{n}] \cdot [\langle \boldsymbol{\epsilon} \rangle_{\mathrm{dam}} \cdot \mathbf{n}] lh \\
&= \sigma_{ij}^{\mathrm{dam}} \epsilon_{ik}^{\mathrm{dam}} n_j n_k lh \\
&= \sigma_{ij}^{\mathrm{dam}} \epsilon_{ik}^{\mathrm{dam}} \delta_{jk} lh = \sigma_{ij}^{\mathrm{dam}} \epsilon_{ij}^{\mathrm{dam}} lh
\end{aligned} \tag{16}$$

where use was made of Eq.(13) and the fact that $\mathbf{t}_{\mathrm{M}}$ equals $\langle \boldsymbol{\sigma} \rangle_{\mathrm{dam}} \cdot \mathbf{n}$ due to equilibrium, see Fig.(18). In the above, δ_{jk} is the Kronecker delta tensor[9]. Comparing the above with the left hand side of Eq.(15) concludes the proof. According to Fig.(17), this proof corresponds to the transition from the equivalent failure band to the crack.

Applying the Hill-Mandel theorem [29] to the active damaged domain Ω_{d}, we can write

$$\frac{1}{|\Omega_{\mathrm{d}}|} \int_{\Omega_{\mathrm{d}}} \boldsymbol{\sigma}_{\mathrm{m}} : \delta \boldsymbol{\epsilon}_{\mathrm{m}} \mathrm{d}\Omega_{\mathrm{d}} = \langle \boldsymbol{\sigma} \rangle_{\mathrm{dam}} : \delta \langle \boldsymbol{\epsilon} \rangle_{\mathrm{dam}} \tag{17}$$

note that the above equation was obtained by considering Ω_{d} as an independent domain. Since a mathematical proof of the above equation is missing, we present numerical evidence of the validity of Eq.(17) in section 4.3. Using Eq.(15), the above becomes

$$\frac{1}{wh} \int_{\Omega_{\mathrm{d}}} \boldsymbol{\sigma}_{\mathrm{m}} : \delta \boldsymbol{\epsilon}_{\mathrm{m}} \mathrm{d}\Omega_{\mathrm{d}} = \frac{1}{w} \mathbf{t}_{\mathrm{M}} \cdot \delta \mathbf{u}_{\mathrm{dam}} \tag{18}$$

---

[9]We have switched the position of the subscript *dam* to superscript when indicial notation was used for convenience of reading.
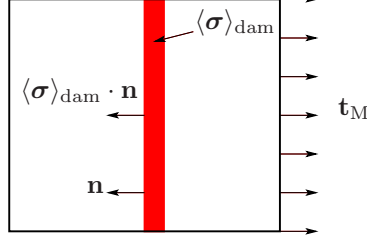
16

Figure 18: Equilibriuum of forces results in $\mathbf{t}_{\mathrm{M}} = \langle \boldsymbol{\sigma} \rangle_{\mathrm{dam}} \cdot \mathbf{n}$. Note that this relation is only used to prove Eq.(15).

The LHS of the above can be written as the difference between the virtual work of the whole micro sample and the linear virtual work. Therefore, we can write

$$\frac{1}{wh} \int_{\Omega_{\mathrm{m}}} \boldsymbol{\sigma}_{\mathrm{m}} : \delta \boldsymbol{\epsilon}_{\mathrm{m}} \mathrm{d}\Omega_{\mathrm{m}} - \frac{1}{wh} \int_{\Omega_{\mathrm{l}}} \boldsymbol{\sigma}_{\mathrm{m}} : \delta \boldsymbol{\epsilon}_{\mathrm{m}} \mathrm{d}\Omega_{\mathrm{l}} = \frac{1}{w} \mathbf{t}_{\mathrm{M}} \cdot \delta \mathbf{u}_{\mathrm{dam}} \tag{19}$$

where Ω_{l} is the linear domain i.e., $\Omega_{\mathrm{l}} = \Omega_{\mathrm{m}} \setminus \Omega_{\mathrm{d}}$.

Using the virtual work equation for the first term of the above equation and the Hill-Mandel condition for the second term, Eq.(19) can be rewritten as

$$\frac{1}{wh} \int_{\Gamma_{\mathrm{m}}} \mathbf{t}_{\mathrm{m}} \cdot \delta \mathbf{u}_{\mathrm{m}} \mathrm{d}\Gamma - \frac{w-l}{w} \langle \boldsymbol{\sigma} \rangle_{\mathrm{lin}} : \delta \langle \boldsymbol{\epsilon} \rangle_{\mathrm{lin}} = \frac{1}{w} \mathbf{t}_{\mathrm{M}} \cdot \delta \mathbf{u}_{\mathrm{dam}} \tag{20}$$

where the homogenized linear stresses and strains $\langle \boldsymbol{\sigma} \rangle_{\mathrm{lin}}$ and $\delta \langle \boldsymbol{\epsilon} \rangle_{\mathrm{lin}}$ are given by

$$\langle \boldsymbol{\sigma} \rangle_{\mathrm{lin}} = \frac{1}{(w-l)h} \int_{\Omega_{\mathrm{l}}} \boldsymbol{\sigma}_{\mathrm{m}} \mathrm{d}\Omega_{\mathrm{l}}$$

$$\delta \langle \boldsymbol{\epsilon} \rangle_{\mathrm{lin}} = \frac{1}{(w-l)h} \int_{\Omega_{\mathrm{l}}} \delta \boldsymbol{\epsilon}_{\mathrm{m}} \mathrm{d}\Omega_{\mathrm{l}} \tag{21}$$

In order to compute the term $\langle \boldsymbol{\sigma} \rangle_{\mathrm{lin}} : \delta \langle \boldsymbol{\epsilon} \rangle_{\mathrm{lin}}$, considering a rectangular homogeneous sample subjected to a traction $\mathbf{t}_{\mathrm{M}}$ on the right edge. The stresses in that sample are given by

$$\langle \boldsymbol{\sigma} \rangle_{xx}^{\mathrm{lin}} = t_{\mathrm{M}}^x, \quad \langle \boldsymbol{\sigma} \rangle_{yy}^{\mathrm{lin}} = 0, \quad \langle \boldsymbol{\sigma} \rangle_{xy}^{\mathrm{lin}} = t_{\mathrm{M}}^y \tag{22}$$

The above equation expressed in matrix-vector notation by using Voigt notation becomes

$$\begin{bmatrix} \langle \boldsymbol{\sigma} \rangle_{xx}^{\mathrm{lin}} \\ \langle \boldsymbol{\sigma} \rangle_{yy}^{\mathrm{lin}} \\ \langle \boldsymbol{\sigma} \rangle_{xy}^{\mathrm{lin}} \end{bmatrix} = \begin{bmatrix} 1 & 0 \\ 0 & 0 \\ 0 & 1 \end{bmatrix} \begin{bmatrix} t_{\mathrm{M}}^x \\ t_{\mathrm{M}}^y \end{bmatrix} \equiv \boldsymbol{\Delta} \mathbf{t}_{\mathrm{M}} \tag{23}$$

or in tensor notation as

$$\langle \boldsymbol{\sigma} \rangle_{\mathrm{lin}} = \boldsymbol{\Delta} \cdot \mathbf{t}_{\mathrm{M}} \tag{24}$$

with the third-order tensor $\boldsymbol{\Delta} = \mathbf{n} \otimes \mathbf{n} \otimes \mathbf{n} + (\mathbf{n} \otimes \mathbf{s} + \mathbf{s} \otimes \mathbf{n}) \otimes \mathbf{s}$, which was firstly given in [17].

17

Now, $\langle\boldsymbol{\sigma}\rangle_{\text{lin}} : \delta\langle\boldsymbol{\epsilon}\rangle_{\text{lin}}$ can be written as

$$
\begin{aligned}
\langle\boldsymbol{\sigma}\rangle_{\text{lin}} : \delta\langle\boldsymbol{\epsilon}\rangle_{\text{lin}} &= \langle\boldsymbol{\sigma}\rangle_{\text{lin}} : \mathbf{D}_{\text{lin}}^{-1} : \delta\langle\boldsymbol{\sigma}\rangle_{\text{lin}} \\
&= (\boldsymbol{\Delta}\cdot\mathbf{t}_{\text{M}}) : [\mathbf{D}_{\text{lin}}^{-1} : (\boldsymbol{\Delta}\cdot\delta\mathbf{t}_{\text{M}})] \\
&= t_p^{\text{M}}\left[\Delta_{ijp}(D_{ijkl}^{\text{lin}})^{-1}\Delta_{klm}\right]\delta t_m^{\text{M}} \\
&= t_p^{\text{M}}(\underbrace{\Delta_{pji}(D_{jikl}^{\text{lin}})^{-1}\Delta_{klm}}_{C_{pm}^{\text{lin}}})\delta t_m^{\text{M}} = \mathbf{t}_{\text{M}}\cdot\mathbf{C}_{\text{lin}}\cdot\delta\mathbf{t}_{\text{M}}
\end{aligned}
\tag{25}
$$

Note that the second-order tensor $\mathbf{C}_{\text{lin}}$ is the projection on the crack plane of the fourth-order compliance tensor $\mathbf{D}_{\text{lin}}^{-1}$ [17]. In the above derivation, the minor symmetry of $\mathbf{D}_{\text{lin}}^{-1}$ was used.

Substituting Eq.(25) into Eq.(20) yields

$$
\frac{1}{wh}\int_{\Gamma_{\text{m}}}\mathbf{t}_{\text{m}}\cdot\delta\mathbf{u}_{\text{m}}\mathrm{d}\Gamma = \frac{w-l}{w}\mathbf{t}_{\text{M}}\cdot\mathbf{C}_{\text{lin}}\cdot\delta\mathbf{t}_{\text{M}} + \frac{1}{w}\mathbf{t}_{\text{M}}\cdot\delta\mathbf{u}_{\text{dam}}
\tag{26}
$$

or

$$
\frac{1}{w}\mathbf{t}_{\text{M}}\cdot\delta\mathbf{u}_{\text{R}} = \frac{w-l}{w}\mathbf{t}_{\text{M}}\cdot\mathbf{C}_{\text{lin}}\cdot\delta\mathbf{t}_{\text{M}} + \frac{1}{w}\mathbf{t}_{\text{M}}\cdot\delta\mathbf{u}_{\text{dam}}
\tag{27}
$$

where the boundary conditions shown in Fig.(4) were adopted to compute the LHS of Eq.(26). In the above, $\mathbf{u}_{\text{R}}$ is the displacement vector of the right edge of the micro sample. The fact that the above holds true for any $\mathbf{t}_{\text{M}}$ yields

$$
\delta\mathbf{u}_{\text{R}} = (w-l)\mathbf{C}_{\text{lin}}\cdot\delta\mathbf{t}_{\text{M}} + \delta\mathbf{u}_{\text{dam}}
\tag{28}
$$

The above can be rewritten as

$$
\delta\mathbf{u}_{\text{R}} = (w-l)\mathbf{C}_0\cdot\delta\mathbf{t}_{\text{M}} + \delta\mathbf{u}_{\text{dam}} + \delta\mathring{\mathbf{u}}_{\text{M}}
\tag{29}
$$

with $\mathbf{C}_0$ being the second-order compliance tensor $\mathbf{C}$ but now evaluated in the undeformed microscale configuration and $\delta\mathring{\mathbf{u}}_{\text{M}}$ given by

$$
\delta\mathring{\mathbf{u}}_{\text{M}} = (w-l)[\mathbf{C}_{\text{lin}} - \mathbf{C}_0]\cdot\delta\mathbf{t}_{\text{M}}
\tag{30}
$$

After a localization band has been formed, the nonlinear part of the total microscale displacement $\mathbf{u}_{\text{R}}$ is assumed to be completely governed by the damage opening $\mathbf{u}_{\text{dam}}$. In other words, $\delta\mathring{\mathbf{u}}_{\text{M}} = 0$, hence Eq.(29) becomes

$$
\delta\mathbf{u}_{\text{R}} = (w-l)\mathbf{C}_0\cdot\delta\mathbf{t}_{\text{M}} + \delta\mathbf{u}_{\text{dam}}
\tag{31}
$$

Using Eq.(14), the equation can be rewritten as follows

$$
\mathbf{u}_{\text{R}} = (w-l)\mathbf{C}_0\cdot\mathbf{t}_{\text{M}} + [\![\mathbf{u}]\!]_{\text{M}} + \mathring{\mathbf{u}}_{\text{dam}}
\tag{32}
$$

The above equation provides the scale transition relation from microscale responses to the macroscale cohesive law (traction $\mathbf{t}_{\text{M}}$ and separation $[\![\mathbf{u}]\!]_{\text{M}}$). Note that for the case in which the micro sample undergoes discrete cracking ($l = 0$), the above reduces to Eq.(17) given in [17].
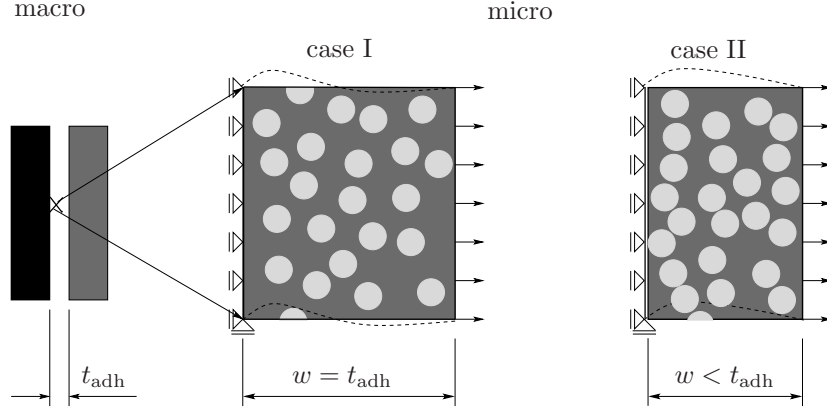
Figure 19: Schematic representation of the homogenization schemes for adhesive cracks with thickness t_{adh}. Case I refers to micro samples having $w = t_{\mathrm{adh}}$ whereas Case II corresponds to micro samples having $w < t_{\mathrm{adh}}$. Periodic BCs are denoted by dashed lines.

4.2. Adhesive cracks

There are two ways in which homogenization schemes for an adhesive crack can be developed, see Fig.(19). According to the first way the micro sample width is chosen to be equal to the thickness of the adhesive crack t_{adh}, referred to as case I in Fig.(19). The authors in [17] have proposed the second approach in which the micro sample width can be smaller than the adhesive crack thickness, referred to as case II in Fig.(19).

4.2.1. Case I

In this case, the micro model covers the complete thickness of the adhesive and crack the displacement of the micro model $\mathbf{u}_{\mathrm{R}}$ can be directly related to the macro jump via

$$\mathbf{u}_{\mathrm{R}} = [\![\mathbf{u}]\!]_{\mathrm{M}} \tag{33}$$

The above is used as BCs for the micro model. After solving the micro model, the macro traction $\mathbf{t}_{\mathrm{M}}$ is given by Eq.(11), see [15, 17].

4.2.2. Case II

In case the adhesive crack t_{adh} is considerably larger than its microstructural constituents and additionally the geometry in the thickness direction is periodic, the homogenization can be applied to a micro model having a width smaller than t_{adh}. The homogenization relation for a cohesive crack, Eq. (32) can be modified for the case of an adhesive crack with thickness t_{adh} as follows. When $w = t_{\mathrm{adh}}$, we have $\mathbf{u}_{\mathrm{R}} = [\![\mathbf{u}]\!]_{\mathrm{M}}$, hence Eq.(32) becomes

$$[\![\mathbf{u}]\!]_{\mathrm{M}} = (t_{\mathrm{adh}} - l)\mathbf{C}_0 \cdot \mathbf{t}_{\mathrm{M}} + [\![\mathbf{u}]\!]_{\mathrm{M}} + \mathring{\mathbf{u}}_{\mathrm{dam}} \tag{34}$$

solving for $\mathring{\mathbf{u}}_{\mathrm{dam}}$ and substituting it into Eq.(32) yields

$$\mathbf{u}_{\mathrm{R}} = (w - t_{\mathrm{adh}})\mathbf{C}_0 \cdot \mathbf{t}_{\mathrm{M}} + [\![\mathbf{u}]\!]_{\mathrm{M}} \tag{35}$$

which provides the homogenization relation between microscale information and the macroscale cohesive law $(\mathbf{t}_{\mathrm{M}}, [\![\mathbf{u}]\!]_{\mathrm{M}})$. Note that this equation resembles Eq.(35) in [17].

Remark 4.1. Homogenization scheme for case I is similar to a homogenization scheme for the bulk material, see Fig.(21). The result obtained with this scheme is referred to as the reference solution. Case II is a homogenization scheme that adjusts the solution of a smaller micro model to match the reference solution. Apparently those homogenization schemes do not use the failure zone averaging technique since the entire response of the micro model is mapped to the macro adhesive crack.

Remark 4.2. Since both homogenization schemes, case I and case II, should yield the same result, one might argue that case I is sufficient. The use of case II, however, offers the following benefits

- a smaller micro sample results in less computational efforts;

- a smaller micro sample could minimize the possibility of microstructural snapback appearances, thus increase the robustness of the method.

4.3. Numerical verification of Equation 17

Equation (17) can be rewritten as $\langle \boldsymbol{\sigma}_m : \delta \boldsymbol{\epsilon}_m \rangle_{\text{dam}} = \langle \boldsymbol{\sigma} \rangle_{\text{dam}} : \delta \langle \boldsymbol{\epsilon} \rangle_{\text{dam}}$ which states that the volume average (over Ω_d) of the microscopic work equals the work done by the averaged (over Ω_d) stresses and strains. Although this equation bears similarity with the Hill-Mandel theorem which is used in standard homogenization schemes, we are currently unable to provide a rigorous proof for it. Instead, we present numerical evidences of the satisfaction of Eq.(17) as shown in Fig.(20). Two samples, of which one has a periodic microstructure and the other has a random microstructure, are analyzed in a uni-axial tension test. The considered material is the three-phase material described in Section 2.1. It is seen that Eq.(17) is practically verified.

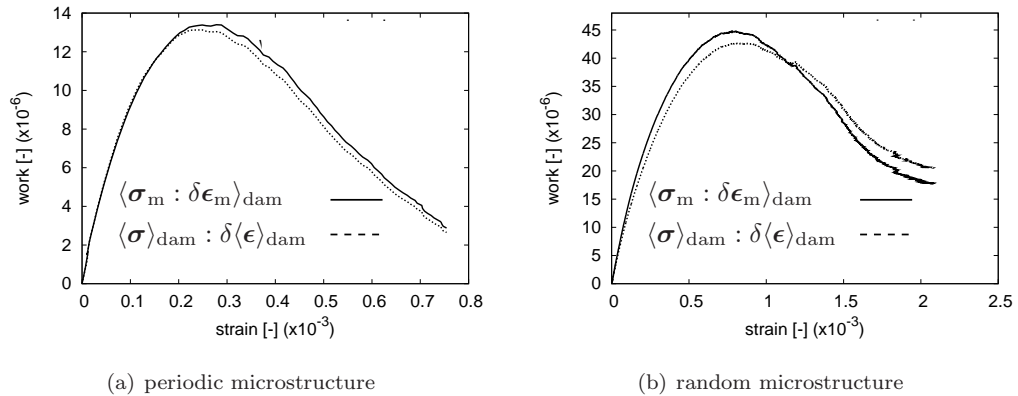(a) periodic microstructure   (b) random microstructure

Figure 20: Numerical evidences of Equation (17).

5. Computational multiscale crack modelling

In the previous sections it has been shown that traction-separation laws which are objective to the micro model size are obtained for materials with simple underlying microstructure and complex random microstructure under various loading conditions including tensile, shear and mixed-mode loading. These cohesive laws can be utilized in two ways, either in sequential homogenization schemes or in semi-concurrent homogenization methods e.g., in a FE^2

Bulk homogenization   Adhesive crack homogenization
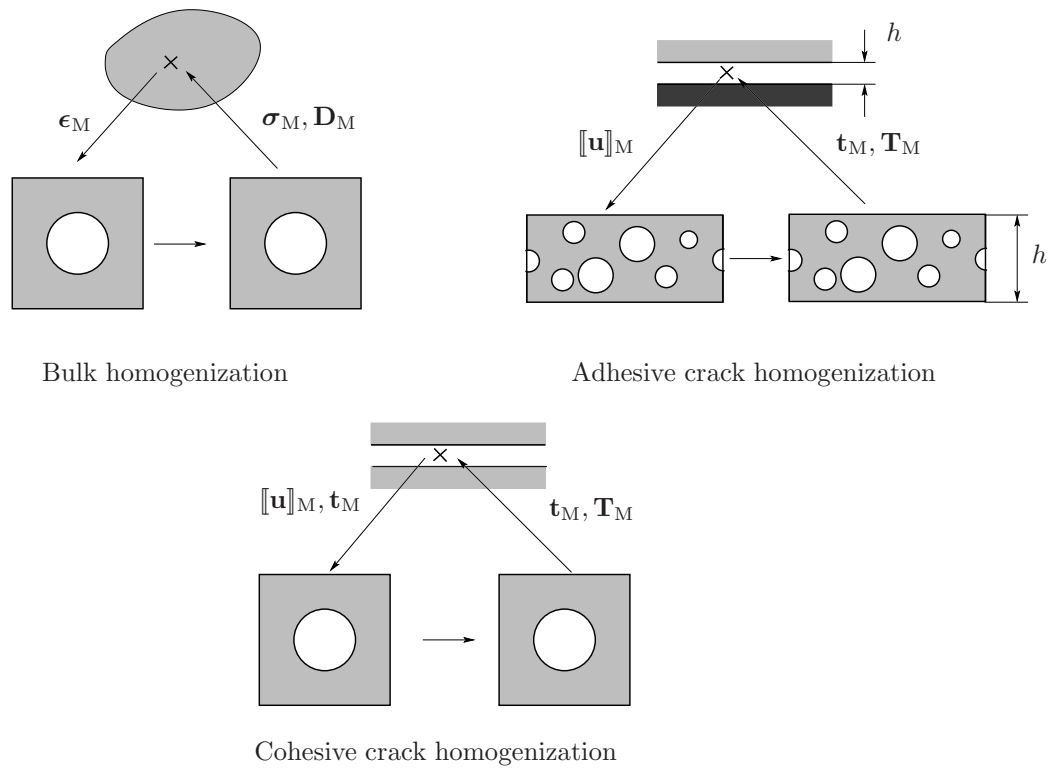
Cohesive crack homogenization

Figure 21: Schematic presentation of bulk homogenization, adhesive crack homogenization and cohesive crack homogenization. The first two cases are typical in the sense of an FE^2 setting: the input for micro FE model is the macro kinematic variable and the output from micro FE model is the work conjugated variable plus its tangent. However, for the cohesive crack, the input for micro FE model includes the opening plus the traction which is solved for simultaneously with the micro displacements.

setting. According to the former, a micro model with properly chosen dimension which is determined, for example, by the RVE's size quantification procedure given in [22, 11, 30], is numerically loaded at different loading conditions, the resulting cohesive laws are snapshot and later on used in a macroscopic FE computations as standard phenomenological constitutive laws[10]. In the spirit of the latter, there is a direct coupling between macro model and micro models. Figure (21) gives an schematic representation of existing computational homogenization methods for bulk material [6, 7, 5, 8], material layers (or interfaces) [13, 15, 14, 12] and cohesive cracks [17]. This section presents computational homogenization schemes for both cohesive and adhesive cracks using the homogenization relations developed in Section 4.

5.1. Adhesive crack homogenization-case I

Homogenization for material layers with $w = t_{adh}$ has firstly been discussed in [12] for small strain problems and later in [13] for the case of finite deformations. In this section, an algorithm for small deformation is given in which a detailed derivation of the tangent matrix is presented. We provide the tangent in a form which is readily incorporated in computer codes (not the case in [13]).

In case of case I adhesive crack homogenization, Fig.(19), the 2×2 cohesive tangent matrix $\mathbf{T}_M$-the tangent in rate format of the macro cohesive law $\delta \mathbf{t}_M = \mathbf{T}_M \delta [\![\mathbf{u}]\!]_M$, is determined as follows.

For illustration assuming that there are only two nodes on the right edge, the traction rate defined in Eq.(11) then becomes

$$
\begin{bmatrix} \delta t_M^x \\ \delta t_M^y \end{bmatrix} = \frac{1}{h} \begin{bmatrix} \delta f_1^{R,x} + \delta f_2^{R,x} \\ \delta f_1^{R,y} + \delta f_2^{R,y} \end{bmatrix} = \frac{1}{h} \begin{bmatrix} 1 & 0 & 1 & 0 \\ 0 & 1 & 0 & 1 \end{bmatrix} \begin{bmatrix} \delta f_1^{R,x} \\ \delta f_1^{R,y} \\ \delta f_2^{R,x} \\ \delta f_2^{R,y} \end{bmatrix} \tag{36}
$$

From the converged linear system of the micro model $\mathbf{K} \delta \mathbf{u} = \delta \mathbf{f}$, the force along the right edge can be written as $\mathbf{K}^* \delta \mathbf{u}_R = \delta \mathbf{f}_R$, so the above becomes

$$
\begin{bmatrix} \delta t_M^x \\ \delta t_M^y \end{bmatrix} = \frac{1}{h} \begin{bmatrix} 1 & 0 & 1 & 0 \\ 0 & 1 & 0 & 1 \end{bmatrix} \begin{bmatrix} K_{11}^* & K_{12}^* & K_{13}^* & K_{14}^* \\ K_{21}^* & K_{22}^* & K_{23}^* & K_{24}^* \\ K_{31}^* & K_{32}^* & K_{33}^* & K_{34}^* \\ K_{41}^* & K_{42}^* & K_{43}^* & K_{44}^* \end{bmatrix} \begin{bmatrix} \delta u_1^{R,x} \\ \delta u_1^{R,y} \\ \delta u_2^{R,x} \\ \delta u_2^{R,y} \end{bmatrix} \tag{37}
$$

where $\mathbf{K}^*$ is the condensed stiffness matrix according to the degrees of freedom of the nodes along the right edge, see [8] for a discussion on this static condensation procedure. Writing the displacements of the right edge in terms of the macro opening displacement, we can write the above as

$$
\begin{bmatrix} \delta t_M^x \\ \delta t_M^y \end{bmatrix} = \frac{1}{h} \underbrace{\begin{bmatrix} 1 & 0 & 1 & 0 \\ 0 & 1 & 0 & 1 \end{bmatrix}}_{\mathbf{M}^T} \begin{bmatrix} K_{11}^* & K_{12}^* & K_{13}^* & K_{14}^* \\ K_{21}^* & K_{22}^* & K_{23}^* & K_{24}^* \\ K_{31}^* & K_{32}^* & K_{33}^* & K_{34}^* \\ K_{41}^* & K_{42}^* & K_{43}^* & K_{44}^* \end{bmatrix} \begin{bmatrix} 1 & 0 \\ 0 & 1 \\ 1 & 0 \\ 0 & 1 \end{bmatrix} \begin{bmatrix} \delta [\![u]\!]_M^x \\ \delta [\![u]\!]_M^y \end{bmatrix} \tag{38}
$$

which obviously shows that the macro cohesive tangent matrix is given by

$$
\mathbf{T}_M = \frac{1}{h} \mathbf{M}^T \mathbf{K}^* \mathbf{M} \tag{39}
$$

---

[10]They are known as micromechanically derived traction-separation laws.

Upon convergence of the micro FE model, the micro stiffness matrix $\mathbf{K}$ is statically condensed out to obtain the right edge micro stiffness matrix $\mathbf{K}^*$ and finally the above equation gives the macro cohesive tangent matrix.

For an iteration of a macroscopic load step, the procedure to compute the macro traction and macro material tangent providing a macro opening displacements $[\![\mathbf{u}]\!]_\mathrm{M}$ is given in Box (1).

Box 1 Adhesive crack homogenization-case I.

1. Given $[\![\mathbf{u}]\!]_\mathrm{M}$
2. Compute $\mathbf{u} = [\![\mathbf{u}]\!]_\mathrm{M}$
3. Apply that displacement $\mathbf{u}$ on the RVE's right edge
4. Solve the RVE problem *
5. Compute the macro traction using Eq.(11)
6. Compute the macro tangent using Eq.(39)
7. Go back to macro model and proceed as in standard FE
8. Upon macro model convergence, update the state of all micro models

* With its state (displacement and internal variables) being reset to its previous converged values.

5.2. Adhesive crack homogenization-case II

Given the macro opening displacements $[\![\mathbf{u}]\!]_\mathrm{M}$, the dimension (w, h) of the micro model and the adhesive thickness t_adh, the system of equations that we want to solve for $\mathbf{u}_\mathrm{m}$ and $\mathbf{t}_\mathrm{M}$ is the following

$$
\begin{aligned}
\mathbf{f}_\mathrm{int}(\mathbf{u}_\mathrm{m}) &= \mathbf{f}_\mathrm{ext}(\mathbf{t}_\mathrm{M}) \\
\mathbf{u}_\mathrm{R}(\mathbf{u}_\mathrm{m}) &= [w - t_\mathrm{adh}]\mathbf{C}_0\mathbf{t}_\mathrm{M} + [\![\mathbf{u}]\!]_\mathrm{M}
\end{aligned}
\tag{40}
$$

in words, solving the micro equilibrium Eq.(40)$_1$ satisfying the homogenization relation Eq.(35). In the above, $\mathbf{f}_\mathrm{int}$ and $\mathbf{f}_\mathrm{ext}$ are the micro internal and external force vector, respectively.

In [17] the above system was solved simultaneously for $\mathbf{u}_\mathrm{m}$ and $\mathbf{t}_\mathrm{M}$. This means that the sought-for macro traction $\mathbf{t}_\mathrm{M}$ is the external force applied on the right edge of the micro sample and Eq.(40)$_2$ is similar to the constraint equation in arc-length control methods. The method can therefore be considered as a *direct force-control computational homogenization* for crack modelling. In the current implementation, we follow a displacement-control procedure, as presented in the sequel.

We model the elastic behavior of the crack as follows. Denoting the thickness of the macro crack t_adh, then the displacement imposed on the micro model reads $\mathbf{u}_\mathrm{R} = (w/t_\mathrm{adh})[\![\mathbf{u}]\!]_\mathrm{M}$[11]. In this way, the macro linear response will be objective to the micro sample size. The proof of the relation $\mathbf{u}_\mathrm{R} = (w/t_\mathrm{adh})[\![\mathbf{u}]\!]_\mathrm{M}$ in the linear regime is as follows. In terms of displacements, Eq.(40)$_2$ is rewritten as

$$
\mathbf{u}_\mathrm{R} = \frac{w - t_\mathrm{adh}}{w}\mathbf{u}_\mathrm{lin} + [\![\mathbf{u}]\!]_\mathrm{M} = \frac{w - t_\mathrm{adh}}{w}\mathbf{u}_\mathrm{R} + [\![\mathbf{u}]\!]_\mathrm{M}
\tag{41}
$$

where the fact that $\mathbf{u}_\mathrm{lin} = \mathbf{u}_\mathrm{R}$ has been used. Solving the above equation for $\mathbf{u}_\mathrm{R}$ yields

$$
\mathbf{u}_\mathrm{R} = \frac{w}{t_\mathrm{adh}}[\![\mathbf{u}]\!]_\mathrm{M}
\tag{42}
$$

---

[11]Note that the tangent given in Eq.(39) in this case is scaled by a factor of w/t_adh.

which concludes the proof.

Whenever the peak at the micro model is observed, say by an appearance of one negative eigenvalue of the macro tangent $\mathbf{T}_{\mathrm{M}}$ as proposed in [31], we switch to the use of the algorithm given in Box (2) as a kind of multiscale constitutive box for the softening branch. As can be seen, the proposed scheme is an *iterative displacement-control computational homogenization scheme* for modelling cracks. It should be emphasized that the iterative procedure converged in the numerical simulations presented here. The appealing point of the iterative scheme compared to the force-control scheme in [17] is that at the micro level, a standard FE procedure is readily reused which facilitates the incorporation of the method in existing FE codes.

Box 2 Iterative displacement-control homogenization for adhesive cracks-case II.

1. Given $[\![\mathbf{u}]\!]_{\mathrm{M}}$ and $\mathbf{u}_{\mathrm{lin}}^0$ *
2. Compute $\bar{\mathbf{u}}_{\mathrm{R}} = [\![\mathbf{u}]\!]_{\mathrm{M}} + \left(\dfrac{w - t_{\mathrm{adh}}}{w} \right) \mathbf{u}_{\mathrm{lin}}^0$
3. Apply that displacement $\bar{\mathbf{u}}_{\mathrm{R}}$ on the RVE's right edge **
4. Solve the RVE problem
5. Compute the macro traction $\mathbf{t}_{\mathrm{M}}$ using Eq.(11)
6. Computing the linear displacement $\mathbf{u}_{\mathrm{lin}} = w\mathbf{C}_0\mathbf{t}_{\mathrm{M}}$, with $\mathbf{C}_0 = \mathbf{\Delta}^{\mathrm{T}}\mathbf{D}_0^{-1}\mathbf{\Delta}$
7. Check convergence
   (a) computing the total micro displacement $\mathbf{u}_{\mathrm{R}} = \dfrac{w - t_{\mathrm{adh}}}{w}\mathbf{u}_{\mathrm{lin}} + [\![\mathbf{u}]\!]_{\mathrm{M}}$
   (b) check $||\mathbf{u}_{\mathrm{R}} - \bar{\mathbf{u}}_{\mathrm{R}}|| < \epsilon\,||\mathbf{u}_{\mathrm{R}}||$. If no, go back to step 2 with $\mathbf{u}_{\mathrm{lin}}^0 = \mathbf{u}_{\mathrm{lin}}$. Else, proceed to step 8
8. Compute the macro material tangent using Eq.(39) and proceed as usual

* Superscript 0 denotes quantities of the previous converged macroscopic load step.
** The left edge is fixed whereas periodic boundary conditions are imposed on the top and bottom edges, see Fig.4.

In Box (2), ϵ is the convergence tolerance and $\mathbf{D}_0$ is the homogenized elasticity matrix which is computed, in a pre-processing step i.e., before the multiscale problem starts, using the standard bulk homogenization method see, for instance, [8].

5.3. Cohesive crack homogenization

The system of equations that needs to be solved for $\mathbf{u}_{\mathrm{m}}$ and $\mathbf{t}_{\mathrm{M}}$, given the macro jump $[\![\mathbf{u}]\!]_{\mathrm{M}}$ and the compatibility displacement $\mathring{\mathbf{u}}_{\mathrm{dam}}$, is

$$
\begin{aligned}
\mathbf{f}_{\mathrm{int}}(\mathbf{u}_{\mathrm{m}}) &= \mathbf{f}_{\mathrm{ext}}(\mathbf{t}_{\mathrm{M}}) \\
\mathbf{u}_{\mathrm{R}}(\mathbf{u}_{\mathrm{m}}) &= [w - l(\mathbf{u}_{\mathrm{m}})]\mathbf{C}_0\mathbf{t}_{\mathrm{M}} + [\![\mathbf{u}]\!]_{\mathrm{M}} + \mathring{\mathbf{u}}_{\mathrm{dam}}
\end{aligned}
\tag{43}
$$

which consists of the micro equilibrium equation Eq.(43)$_1$ and the homogenization relation Eq.(32).

Similar to the case of adhesive cracks presented in the previous section, the above system is solved by an iterative displacement-control procedure as given in Box (3). This is not only because both adhesive and cohesive cracks can be handled in a common displacement-control framework but also due to the dependency of the localization band width l on the micro displacements $\mathbf{u}_{\mathrm{m}}$. Since we mainly focus on the extraction of objective cohesive laws from the responses of the micro sample, the crack initiation/propagation is based on the macroscopic maximum principle stress criterion and the crack growth direction is computed based upon the nonlocal stresses at the crack tip, see for instance [32], as conventionally adopted in monoscale crack modelling. It should be noticed that in [20], the crack initiation and growth

direction have been based on microscopic responses. The iterative displacement-control procedure for cohesive cracks is summarized in Box (3).

Box 3 Iterative displacement-control homogenization for cohesive cracks.

1. Run macro model until $\sigma_I \geq \alpha\sigma_{\text{ult}}$, $\alpha \approx 1.0$
2. Insert a crack segment with a proper direction
    (a) Initialize 2 micro models associated to 2 Gauss points on the crack segment
    (b) Loading those 2 micro models up to σ_I via load control *
    (c) Computing the initial damage opening $\mathring{\mathbf{u}}_{\text{dam}}$
3. Given $[\![\mathbf{u}]\!]_{\text{M}}$, $\mathbf{u}_{\text{lin}}^0$ and l^0 **
    (a) Compute $\bar{\mathbf{u}}_{\text{R}} = [\![\mathbf{u}]\!]_{\text{M}} + \mathring{\mathbf{u}}_{\text{dam}} + \left(\dfrac{w - l^0}{w}\right)\mathbf{u}_{\text{lin}}^0$
    (b) Apply that displacement $\bar{\mathbf{u}}_{\text{R}}$ on the RVE's right edge
    (c) Solve the RVE problem
    (d) Compute the macro traction $\mathbf{t}_{\text{M}}$ using Eq.(11)
    (e) Compute the linear displacement $\mathbf{u}_{\text{lin}} = w\mathbf{C}_0\mathbf{t}_{\text{M}}$, with $\mathbf{C}_0 = \mathbf{\Delta}^{\text{T}}\mathbf{D}_0^{-1}\mathbf{\Delta}$
    (f) Computing the new localization band width $l = |\Omega_{\text{d}}|/h$
    (g) Check convergence
        i. computing the total micro displacement $\mathbf{u}_{\text{R}} = [\![\mathbf{u}]\!]_{\text{M}} + \mathring{\mathbf{u}}_{\text{dam}} + \dfrac{w - l}{w}\mathbf{u}_{\text{lin}}$
        ii. check $||\mathbf{u}_{\text{R}} - \bar{\mathbf{u}}_{\text{R}}|| < \epsilon\,||\mathbf{u}_{\text{R}}||$. If no, go back to step 3b with $\bar{\mathbf{u}}_{\text{R}} = \mathbf{u}_{\text{R}}$. Else, proceed to step 4
4. Compute the macro material tangent using Eq.(39) and proceed as usual.

* This is achieved by subdividing σ_I into a number of small load steps.
** Superscript 0 denotes quantities of the previous converged macroscopic load step.

In Box (3), the macroscopic maximum principal stress was denoted by σ_I and σ_{ult} is the ultimate strength of the material which is, in a multiscale framework, the ultimate load of the microscale model (this quantity is currently determined by loading first the micro sample in a pre-processing step). The crack initiation equation $\sigma_I \geq \alpha\sigma_{\text{ult}}$, $\alpha \approx 1.0$, as proposed by [17], ensures that the time continuity condition [33] is fulfilled (thus enhance the robustness of the crack growth algorithm) and more importantly the solution procedure for the micro models will not diverge. The proposed algorithm can be incorporated in any numerical codes with the capacity to model cracks e.g., PUM-based (Partition of Unity) enrichment finite elements [34, 32].

The macroscopic bulk behaves elastically with effective properties computed based on numerical homogenization applied to the micro samples. Given the strain vector, the macroscopic stress vector is thus given by

$$\boldsymbol{\sigma}_{\text{M}} = \mathbf{D}_0\boldsymbol{\epsilon}_{\text{M}} \tag{44}$$

5.4. Some algorithmic aspects

For a robust and efficient implementation of the proposed multiscale framework, some algorithmic aspects have to be considered. Since in [17] related details have already been given, in this section we only discuss some techniques in order to have a robust multiscale scheme. It is likely that in a FE^2 simulation divergence of one (or more) micro problem(s) will occur. Straightforward remedies of this problem could be either *(i)* resolving the macro load step which led to a micro divergence with a smaller step size or *(ii)* sub-stepping the imposed displacement $\bar{\mathbf{u}}_{\text{R}}$ into a number of smaller steps. In the current implementation, we are using the latter option. The sub-stepping scheme discussed in

[35] could be another option worth to be considered. Needless to say, a comparison study, say by means of numerical experiments, of those techniques would be necessary to choose the most efficient one and is a topic of further study. It is emphasized that the proposed scheme cannot deal with the snapback behavior occurring at the micro models[12]. Macroscopic snapback can however be handled by, for instance, the energy-based arc-length control given in [36].

6. Benchmark problems

6.1. Adhesive crack

Figure (22) gives a benchmark problem for verifying the proposed multiscale scheme. The aim is to check whether the macroscopic response is objective to the micro sample size. The material parameters of the micro model are given in section 2.2. The macro bulk material is an elastic material with Young's modulus of 25000 N/mm^2 and Poisson's ratio of zero. Note that in contrary to the cohesive crack, for an adhesive crack, the macroscopic bulk is not related to the microstructure of the adhesive crack. A plane stress condition is assumed for the macro model and the micro models as well. The thickness of the interface t_{adh} is assumed to be 40 mm.
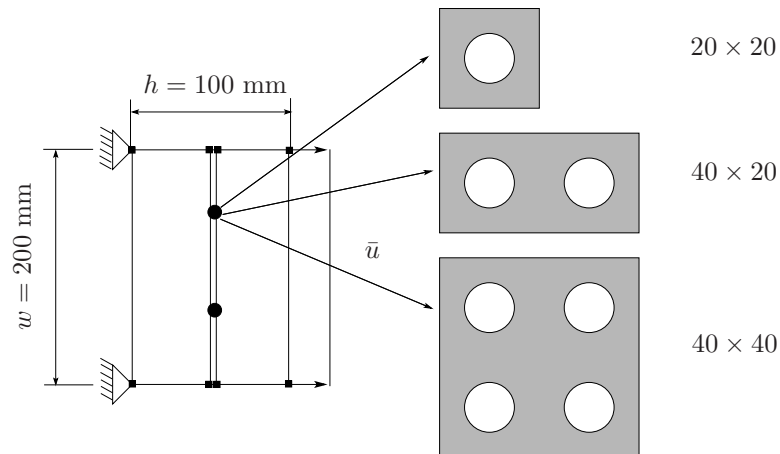
Figure 22: Crack modelling by interface elements. Cohesive law extracted from micro FE computations whereas bulk material obeys a phenomenological linear elastic constitutive law.

Using the case I adhesive crack homogenization scheme given in Box (1), the macroscopic load-displacement diagrams corresponding to the 40×20 and 40×40 samples (note that the sample 20×20 cannot be used in this case) are given in Fig.(23)-left. The responses are obviously objective to the micro sample size. Figure (23)-right presents the macroscopic responses for all three samples using the new iterative homogenization scheme given in Box (2). The results are practically coincident. It has been observed that for one macroscale Newton-Raphson iteration, the iterative scheme (Box (2)) has converged in two to four iterations with a tolerance of $\epsilon = 10^{-4}$. Far from the peak, when the contribution of elastic processes becomes negligible, the number of required iterations is usually only one or two.

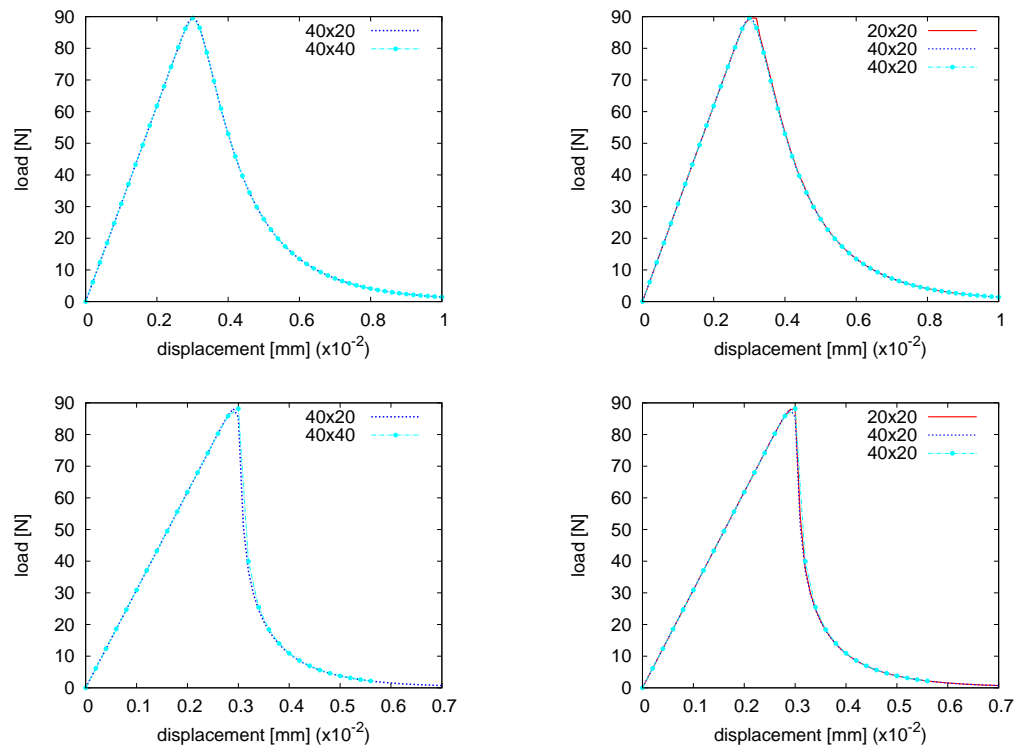[12]It is however noticed that snapback is not likely to occur in the micro samples.

Figure 23: Adhesive crack benchmark problem: macroscopic load displacement ($\bar{u}$) curves obtained with the standard scheme (left) and the iterative displacement-control homogenization scheme (right). Top figures correspond to ductile fracture ($\beta = 3000$) and the bottom one for brittle fracture ($\beta = 5000$).

6.2. Cohesive crack

Figure (24) depicts a simple crack growth simulation problem, a bar in uniaxial tension which is discretized by 3 four-node quadrilateral elements. Refer to section 2.2 for the material parameters of the micro models (except $\beta = 1000$). When the maximum principal stress in the bar exceeds 0.4475 MPa, 95% the micro model ultimate load σ_{ult}, a vertical crack is, due to symmetry, inserted in the middle element. The behavior of that crack is governed by one of the three microstructures as shown in Fig.(24). A plane stress condition is assumed for the micro models. The aim of the example is to verify the objectivity of the macroscopic responses with respect to the utilized microstructures.
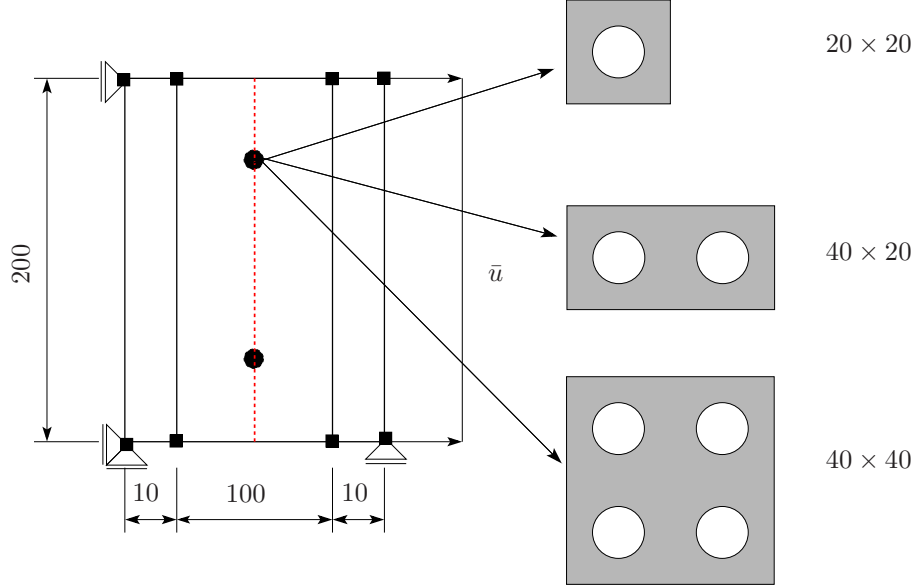
Figure 24: Cohesive crack modelling by PUM with cohesive law coming from microscopic FE computations. Due to symmetry, a vertical crack (dashed line) is inserted in the middle element upon violation of the fracture criterion. All units are in mm.

Figure (25) presents the macroscopic load-displacement ($\bar{u}$) curves which are clearly independent of the microstructures used to obtain the homogenized macroscopic cohesive laws shown in the right figure. Note that since the macro crack was inserted slightly before the ultimate load of the micro models, the homogenized cohesive laws are not initially rigid as conventional cohesive models. We have also analyzed the effect of the α parameter used in the crack initiation/propagation criterion $\sigma_I \geq \alpha\sigma_{\text{ult}}$ on the overall macroscopic response. The result, reported in Fig.(26) for the 20×20 sample, shows that there is hardly any considerable effect of this parameter on the overall behavior of the macroscopic sample. The observed load drops in the macroscopic load-displacement diagrams are due to the fact that the microscopic dimensions are of the same magnitude with the macroscopic one.

6.3. Verification of the method against DNS

To verify the proposed multiscale method, let us consider the example shown in Fig.(27) of which the solution obtained with the multiscale model is going to be compared with the one obtained with the DNS . The shaded region is modelled as a damageable material (material parameters can be found in section 2.2 except $\beta = 3000$) whereas the rest behaves elastically. The finite element mesh of the DNS model is given in Fig.(28).

In case that the shaded region represents the microstructure of a material layer of thickness $t_{\text{adh}} = 20$ mm, the finite element mesh for the multiscale model (adhesive crack-case I) is given in Fig.(29). The adequacy of the multiscale
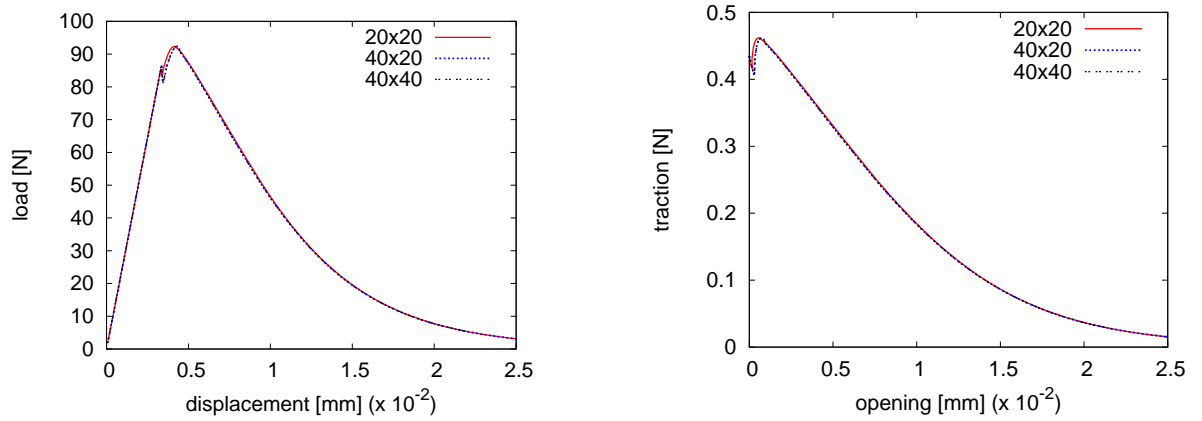
28

Figure 25: Cohesive crack problem: objective macroscopic load-displacement diagrams obtained with various microstructures (left) and homogenized traction-opening laws (right).
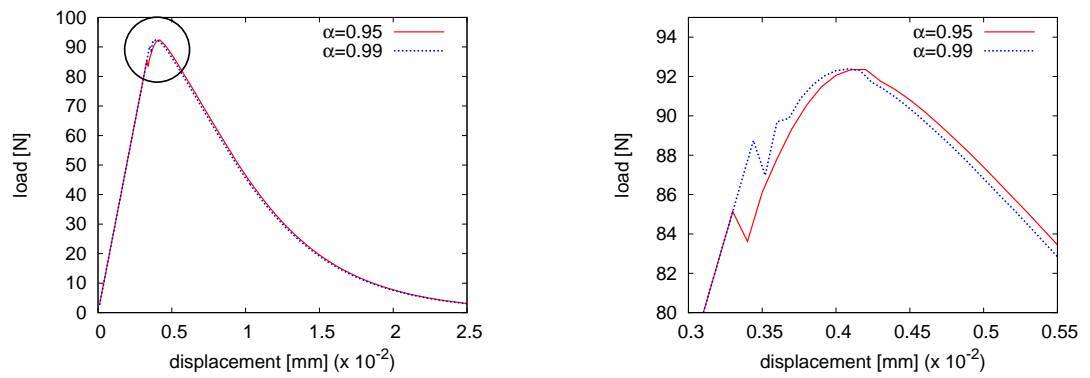

Figure 26: Cohesive crack problem: consequences of the crack initiation moment on the overall macroscopic response (left) and close-up view (right).
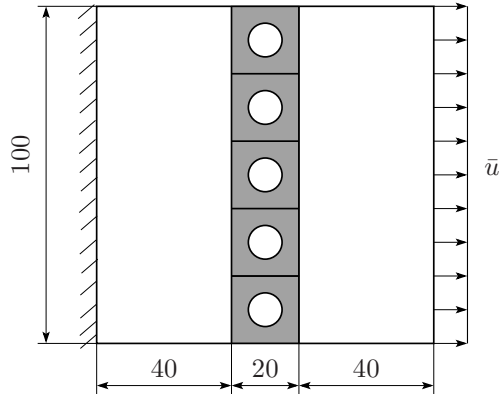
Figure 27: Verification test: geometry and boundary conditions. All units are in mm.

solution can be judged from Fig.(30) which presents the comparison of load-displacement curves between the multiscale (denoted as FE2) simulation and the DNS. The multiscale solution captures the peak load and later stages well with a much lower computational time (in this particular example the DNS simulation time is approximately 10 times the one of the multiscale method).
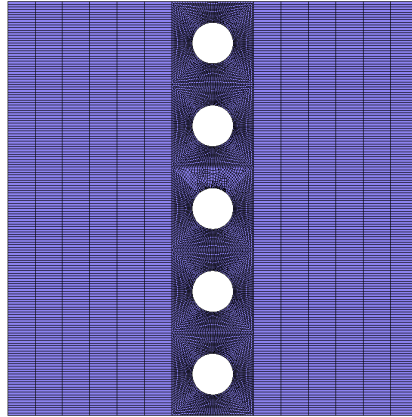

Figure 28: Verification test-DNS model: finite element discretization (14024 bilinear elements).

For the multiscale cohesive crack homogenization scheme, the finite element discretizations for the macro and micro models are presented in Fig.(31). The adequacy of the multiscale solution can be judged from Fig.(32) which compares the load-displacement curve of the multiscale model to that of the DNS model. The multiscale solution captures the peak load and later stages well. The DNS simulation requires approximately 6 times the computation time of the multiscale model. It is emphasized that for problems in which the crack path is not known a priori, the use of DNS is impractical since the microstructure has to be resolved everywhere which leads to prohibitive computational expense.
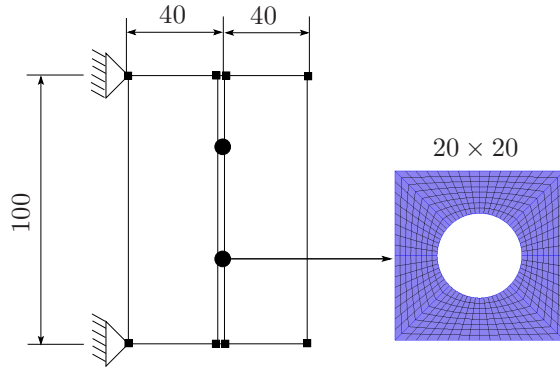
Figure 29: Verification test-Multiscale model (adhesive crack): finite element discretization (2 bilinear elements and one linear interface element) of the coarse scale model and a typical fine scale model (512 bilinear elements).
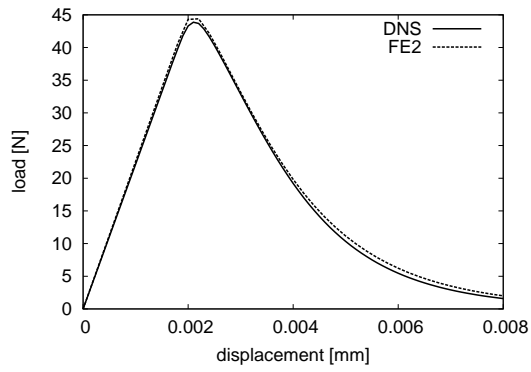

Figure 30: Verification test: comparison of load-displacement curves between the DNS and the multiscale-case I adhesive crack scheme.
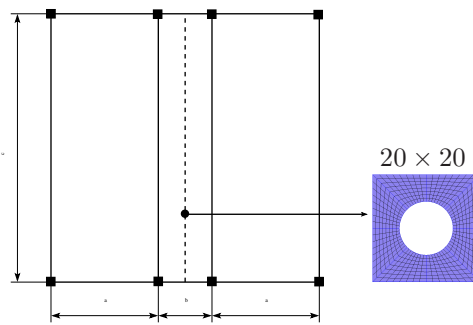

Figure 31: Verification test-Multiscale model (cohesive crack): finite element discretization (3 bilinear elements) of the coarse scale model and a typical fine scale model (512 bilinear elements).
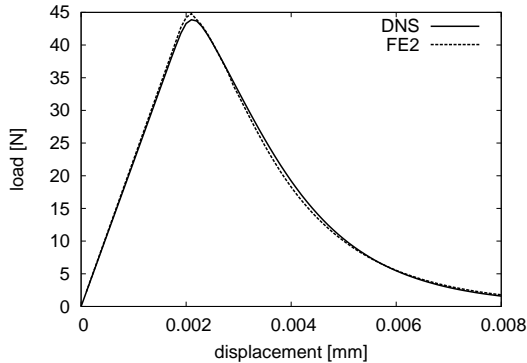
Figure 32: Verification test: comparison of load-displacement curves between the DNS and the multiscale cohesive crack scheme.

7. Conclusions

In this contribution macroscopic cohesive laws (both mode I and mode II), which are independent of the micro sample size, were obtained for quasi-brittle materials with a random heterogeneous microstructure under various loading conditions for both cohesive and adhesive cracks. This was achieved by extracting only the active inelastic responses occuring in the micro sample (rather than the whole responses in the micro sample as in standard homogenization schemes) to determine the equivalent homogenized macroscopic ones. The paper confirmed the existence of an RVE for quasi-brittle materials with a random microstructure that exhibits damage in a smeared average fashion under tensile and shear loadings.

Using the Hill's energetic equivalence condition in combination with the proposed failure zone averaging scheme, homogenization relations for both macroscopic adhesive and cohesive cracks were obtained for materials exhibiting diffusive damage. The proposed homogenization scheme can be considered as an aggregation of a micro localization band to a macro discontinuous crack in an energetically equivalent manner. The homogenization scheme was implemented in a standard strain-driven FE^2 framework and successfully verified by three simple numerical examples. The proposed homogenization scheme is objective with respect to the micro model size apart being independent of macro and micro finite element discretizations. The method has been verified by comparing it with a direct numerical simulation.

Future work would be *(i)* extension of the currently proposed energetic equivalence conditions to the case in which there are simultaneously diffusive damage and discrete cracking e.g., decohesion of material interfaces occurring in the microstructure, *(ii)* a statistical analysis of the representativeness of the macroscopic cohesive laws of samples subjected to mixed mode loading and *(iii)* a study on the effect of volume fraction of the aggregates, shape of the aggregates on the resulting cohesive laws.

[1] T. Belytschko and J.H. Song. Coarse-graining of multiscale crack propagation. *International Journal for Numerical Methods in Engineering*, 81(5):537–563, 2010.

[2] O. van der Sluis, P. J. G. Schreurs, W. A. M. Brekelmans, and H. E. H. Meijer. Overall behaviour of heterogeneous elastoviscoplastic materials: effect of microstructural modelling. *Mechanics of Materials*, 32(8):449–462, August 2000.

[3] P. M. Suquet. Local and global aspects in the mathematical theory of plasticity. In A. Sawczuk and G. Bianchi, editors, *Plasticity today: modelling, methods and applications*, pages 279–310, London, 1985. Elsevier.

[4] I. M. Gitman, H. Askes, and L. J. Sluys. Coupled-volume multi-scale modelling of quasi-brittle material. *European Journal of Mechanics - A/Solids*, 27(3):302–327, 2007.

[5] F. Feyel. A multilevel finite element method (fe2) to describe the response of highly non-linear structures using generalized continua. *Computer Methods in Applied Mechanics and Engineering*, 192:3233–3244, 2003.

[6] R.J.M. Smit, W.A.M. Brekelmans, and H.E.H. Meijer. Prediction of the mechanical behavior of nonlinear heterogeneous systems by multi-level finite element modeling. *Computer Methods in Applied Mechanics and Engineering*, 55:181–192, 1998.

[7] S. Ghosh, K. Lee, and S. Moorthy. Two scale analysis of heterogeneous elastic-plastic materials with asymptotic homogenization and Voronoi cell finite element model. *Computer Methods in Applied Mechanics and Engineering*, 132:63–116, 1996.

[8] V. Kouznetsova, W. A. M. Brekelmans, and F. P. T. Baaijens. An approach to micro-macro modeling of heterogeneous materials. *Computational Mechanics*, 27(1):37–48, 2001.

[9] M. G. D. Geers, V. G. Kouznetsova, and W. A. M. Brekelmans. Multi-scale computational homogenization: Trends and challenges. *Journal of Computational and Applied Mathematics*, 234(7):2175–2182, 2010.

[10] A. Abdulle and A. Nonnenmacher. A short versatile finite element multiscale code for homogenization problems. *Computer Methods in Applied Mechanics and Engineering*, 198(37-40):2839–2859, 2009.

[11] I.M. Gitman, H. Askes, and L.J. Sluys. Representative volume: Existence and size determination. *Engineering Fracture Mechanics*, 74(16):2518–2534, 2007.

[12] K. Matouš, M. G. Kulkarni, and P. H. Geubelle. Multiscale cohesive failure modeling of heterogeneous adhesives. *Journal of the Mechanics and Physics of Solids*, 56(4):1511–1533, 2008.

[13] C. B. Hirschberger, S. Ricker, P. Steinmann, and N. Sukumar. Computational multiscale modelling of heterogeneous material layers. *Engineering Fracture Mechanics*, 76(6):793–812, 2009.

[14] M. G. Kulkarni, P. H. Geubelle, and K. Matouš. Multi-scale modeling of heterogeneous adhesives: Effect of particle decohesion. *Mechanics of Materials*, 41(5):573–583, 2009.

[15] M.V. Cid Alfaro, A.S.J. Suiker, C.V. Verhoosel, and R. de Borst. Numerical homogenization of cracking processes in thin fibre-epoxy layers. *European Journal of Mechanics - A/Solids*, 29(2):119–131, 2010.

[16] C. V. Verhoosel, J. J. C. Remmers, and M. A. Gutiérrez. A partition of unity-based multiscale approach for modelling fracture in piezoelectric ceramics. *International Journal for Numerical Methods in Engineering*, 2009.

[17] C. V. Verhoosel, J. J. C. Remmers, M. A. Gutiérrez, and R. de Borst. Computational homogenisation for adhesive and cohesive failure in quasi-brittle solids. *International Journal for Numerical Methods in Engineering*, 2010.

[18] T. Belytschko, S. Loehnert, and J.H. Song. Multiscale aggregating discontinuities: A method for circumventing loss of material stability. *International Journal for Numerical Methods in Engineering*, 73(6):869–894, 2008.

[19] A. Hund and E. Ramm. Locality constraints within multiscale model for non-linear material behaviour. *International Journal for Numerical Methods in Engineering*, 70(13):1613–1632, 2007.

[20] T.J. Massart and B.C.N. Mercatoris. Assessment of periodic homogenisation-based multiscale computational schemes for quasi-brittle structural failure. *International Journal for Multiscale Computational Engineering*, 7(2):153–170, 2009.

[21] V.P. Nguyen, O. Lloberas Valls, M. Stroeven, and L.J. Sluys. On the existence of representative volumes for softening quasi-brittle materials-A failure zone averaging scheme. *Computer Methods in Applied Mechanics and Engineering*, 2010. In Press, Corrected Proof.

[22] M. Stroeven, H. Askes, and L. J. Sluys. Numerical determination of representative volumes for granular materials. *Computer Methods in Applied Mechanics and Engineering*, 193(30-32):3221–3238, 2004.

[23] R. H. J. Peerlings, R. de Borst, W. A. M. Brekelmans, and J. H. P. de Vree. Gradient enhanced damage for quasi-brittle materials. *International Journal for Numerical Methods in Engineering*, 39:3391–3403, 1996.

[24] J. Lemaitre. *A course on damage mechanics.* Springer-Verlag, 1996.

[25] J. Mazars and G.Pijaudier-Cabot. Continuum damage theory - application to concrete. *Journal of Engineering Mechanics Division ASCE*, 115:345–365, 1989.

[26] T.I. Zohdi and P. Wriggers. *Introduction to computational micromechanics.* Springer-Verlag, 2005.

[27] K. Matouš and P.H. Geubelle. Multiscale modelling of particle debonding in reinforced elastomers subjected to finite deformations. *International Journal for Numerical Methods in Engineering*, 65:190–223, 2006.

[28] I.M. Gitman, H. Askes, L.J. Sluys, and O. Lloberas. The concept of representative volume for elastic, hardening and softening materials. In *Proceedings of XXXII International Summer School-Conference "Advance problems in Mechanics"*, pages 180–184, Saint Petersburg (Repino) Russia, 2004.

[29] R. Hill. On constitutive macro-variables for heterogeneous solids at finite strain. *Proc. R. Soc. Lond.*, 326:131–147, 1972.

[30] C. Pelissou, J. Baccou, Y. Monerie, and F. Perales. Determination of the size of the representative volume element for random quasi-brittle composites. *International Journal of Solids and Structures*, 46(14-15):2842–2855, 2009.

[31] T. J. Massart, R. H. J. Peerlings, and M. G. D. Geers. An enhanced multi-scale approach for masonry wall computations with localization of damage. *International Journal for Numerical Methods in Engineering*, 69(5):1022–1059, 2007.

[32] G. N. Wells and L. J. Sluys. A new method for modelling cohesive cracks using finite elements. *International Journal for Numerical Methods in Engineering*, 50(12):2667–2682, 2001.

[33] K. D. Papoulia, C.H. Sam, and S. A. Vavasis. Time continuity in cohesive finite element modeling. *International Journal for Numerical Methods in Engineering*, 58(5):679–701, 2003.

[34] N. Moës, J. Dolbow, and T. Belytschko. A finite element method for crack growth without remeshing. *International Journal for Numerical Methods in Engineering*, 46(1):131–150, 1999.

[35] D.D. Somer, E.A. de Souza Neto, W.G. Dettmer, and D. Perić. A sub-stepping scheme for multi-scale analysis of solids. *Computer Methods in Applied Mechanics and Engineering*, 198(9-12):1006–1016, February 2009.

[36] C. V. Verhoosel, J. J. C. Remmers, and M. A. Gutiérrez. A dissipation-based arc-length method for robust simulation of brittle and ductile failure. *International Journal for Numerical Methods in Engineering*, 77(9):1290–1321, 2009.